https://doi.org/10.5194/egusphere-2026-4642
Preprint. Discussion started: 7 August 2026

Impact of the NGGM and MAGIC future satellite gravity missions for scientific applications and operational services

Julia Pfeffer[1], Benoît Meyssignac[2], Rory Bingham[3], Alejandro Blazquez[2], Marie Bouih[1], Carla Braitenberg[4], Luca Brocca[5], Henryk Dobslaw[6], Ramiro Ferrari[1], Ehsan Forootan[7], Helena Gerdener[8], Muhammad Tahir Javed[4], Laura Jensen[6], Volker Klemann[6], Anna Kremer[9,8], Jürgen Kusche[8], Gilles Larnicol[1], Muhammad Usman Liaqat[5], Francesco Leopardi[5], Elisavet-Maria Mamagiannou[10], Gerardo Maurizio[4], Roland Pail[11], Isabelle Panet[9], Thomas Papanikolaou[10], Peyman Saemian[12], Ingo Sasgen[13,14], Maike Schumacher[7], Marius Schlaak[11], Linus Shihora[6], Alireza Sobouti[12], Nico Sneeuw[12], Mohamad J. Tourian[12], Dimitrios Tsoulis[10], Georgios Vergos[10], Bert Wouters[15], Fan Yang[7], Ilias Daras[16]

[1] Magellium, Ramonville - Saint - Agne, 31750, France
[2] CNES, Toulouse, 31400, France
[3] University of Bristol, Bristol, BS8 1QU, United Kingdom
[4] University of Trieste, Trieste, 34127, Italy
[5] Research Institute for Geo-Hydrological Protection, National Research Council, Perugia, 06128, Italy
[6] GFZ Helmholtz Centre for Geosciences, Potsdam, 14473, Germany
[7] University of Aalborg, Aalborg, 9220, Denmark
[8] University of Bonn, Bonn, 53115, Germany
[9] Institut de Physique du Globe de Paris, Paris, 75005, France
[10] Aristotle University of Thessaloniki, Thessaloniki, 54124, Greece
[11] Technical University of Munich, Munich, 80333, Germany
[12] Institute of Geodesy, University of Stuttgart, Stuttgart, 70174, Germany
[13] Alfred Wegener Institute Helmholtz Centre for Polar and Marine Research, Bremerhaven, 27570, Germany
[14] Institute of Geography, University of Augsburg, Augsburg, 86159, Germany.
[15] Delft University of Technology, Deft, 2628 CN, The Netherlands
[16] European Space Research and Technology Center, European Space Agency, Noordwijk, 2201 AZ, The Netherlands

Correspondence to: Julia Pfeffer (julia.pfeffer@magellium.fr)

Abstract. The ESA SING project evaluates the added value of the Next Generation Gravity Mission (NGGM) and the Mass-change and Geoscience International Constellation (MAGIC) for scientific applications and operational services in hydrology, oceanography, glaciology, climate science, solid Earth science, and geodesy. Using a closed-loop simulation framework that incorporates realistic instrumental, tidal and aliasing errors, synthetic gravity observations were generated to assess the capability of future satellite gravity missions to monitor mass variations in the atmosphere, oceans, hydrosphere, cryosphere, and solid Earth. The enhanced spatial and temporal resolution of NGGM and MAGIC substantially improves the monitoring and prediction of hydrological extremes, including floods and droughts, while estimates of total water storage anomalies, combined with complementary in situ observations and hydrological models, enable improved estimation of key variables of the continental water cycle, including precipitation and total drainable water storage. The improved resolution, accuracy, and

https://doi.org/10.5194/egusphere-2026-4642
Preprint. Discussion started: 7 August 2026

temporal coverage of gravity observations are also critical for detecting climate-driven changes in the Atlantic Meridional Overturning Circulation (AMOC). Enhanced monitoring of mass changes in glaciers and ice sheets enable the detection of more rapid melt and accumulation events at finer spatial scales. Improved closure of sea-level and energy budgets is achieved through more accurate observations of mass redistribution at smaller spatial and temporal scales. In solid Earth applications, NGGM and MAGIC increase sensitivity to co-seismic and post-seismic deformation associated with smaller earthquakes while reducing data latency, thereby strengthening geohazard assessment and early warning capabilities. In geodesy, the missions support improved gravity field and geoid modelling, contributing to the realization and temporal evolution of the International Height Reference Frame (IHRF) and to more accurate precise orbit determination. Overall, the ESA SING results provide strong evidence of the scientific and societal benefits of NGGM and MAGIC to prepare the integration of future Earth Observation data into operational services.

1 Introduction

The GRACE (Gravity Recovery and Climate Experiment; Tapley et al., 2004) and GRACE-FO (GRACE Follow-On; Landerer et al., 2020) missions fundamentally advanced the observation of mass transport within the Earth system. Time-lapse gravity field solutions derived from these missions enabled global monitoring of water mass changes in the atmosphere, oceans, hydrosphere, and cryosphere, and provided unique insights into solid Earth deformation across multiple spatial and temporal scales (Chen et al., 2022; Tapley et al., 2019). Satellite gravimetry has become indispensable for quantifying sea-level rise (Bouih et al., 2025), ocean heat uptake (Marti et al., 2022; Meyssignac et al., 2019), the mass balance of ice sheets (Sasgen et al., 2019, 2020) and glaciers (Wouters et al., 2019), and for detecting and characterizing extreme events such as floods (Kusche et al., 2016), droughts (Forootan et al., 2024; Gerdener, 2024), and major earthquakes (Panet et al., 2007, 2018). The GRACE and GRACE-FO missions also advanced the modeling of physical heights, gravity, and the geoid (Vergos et al., 2024) and played a key role in the realization of the International Height Reference Frame (IHRF; Sánchez et al., 2024).

Continued progress toward higher-accuracy, higher-resolution, and near-real-time gravity field products is required to support emerging scientific applications and time-critical decision-making in climate services, natural hazard response, and water-resource management (Pail et al., 2015). To address these evolving requirements, the Mass change And Geosciences International Constellation (MAGIC) has been designed as a joint ESA–NASA mission (European Space Agency et al., 2020; Heller-Kaikov et al., 2023; Daras et al., 2024). The mission responds to four primary objectives (Daras et al., 2024): (i) the continuity of the long-term gravity record, (ii) improved spatial resolution, (iii) improved temporal resolution, and (iv) reduced data latency. MAGIC fulfils these objectives through a dual-pair architecture arranged in a quasi-Bender constellation, in which complementary orbit geometries increase the spatial and temporal resolution, reduce aliasing errors, and improve signal recovery. The constellation comprises two satellite pairs: GRACE-C (GRACE-Continuity), developed by NASA/DLR, will operate in a near-polar orbit at approximately 500 km altitude to ensure seamless continuation of the GRACE and GRACE-

https://doi.org/10.5194/egusphere-2026-4642
Preprint. Discussion started: 7 August 2026

FO record, while the he NGGM (Next Generation Gravity Mission) pair, developed by ESA, will operate in an inclined (70 degrees), lower-altitude (~400 km) controlled orbit (Daras, 2026). Following completion of GRACE-C operations, NGGM will continue measurements with reduced coverage at high latitudes, due to the inclination of the orbit. Performance evaluations of MAGIC and NGGM mission scenarios demonstrated substantial improvements relative to a single GRACE-like pair in the spatiotemporal resolution and accuracy of Level-2 and Level-3 gravity field products (Daras et al., 2024; Heller-Kaikov et al., 2023), encompassing time-lapse estimates of the gravity field, expressed as Stokes coefficients of the geopotential, as well as gridded surface mass anomalies, expressed as ice mass changes (Gt) over glaciated regions, terrestrial water storage anomalies (TWSA) over continental areas and ocean bottom pressure (OBP) changes over the oceans.

The ESA SING project assesses the impact of the NGGM and MAGIC missions on higher-level (Level 4) geophysical products generated by data assimilation and data fusion across multiple Earth-system domains. Performance assessments, based on synthetic NGGM and MAGIC observations generated within a closed-loop simulator, including rigorous uncertainty quantification, examine how advances in gravity field observations enhance the monitoring and understanding of key Earth system processes and contribute to the development of future operational services. This paper reviews the principal outcomes of the ESA SING project, highlighting the expected scientific and societal benefits of NGGM and MAGIC. The results demonstrate that next-generation satellite gravimetry can strengthen freshwater and drought monitoring, improve flood forecasting and water-resource management, advance climate-change assessment, enhance the monitoring of sea-level rise and cryospheric change, support the detection of large-scale climate tipping elements such as the Atlantic Meridional Overturning Circulation (AMOC), improve observations of earthquake-related mass redistribution, and contribute to more accurate geodetic reference frames and satellite orbit determination. Together, these advances illustrate the growing role of satellite gravimetry as a key component of the global Earth observation system for both scientific research and operational applications.

2 Synthetic observations of future satellite gravity missions

Synthetic observations of the gravity field are generated for three mission configurations (GRACE-C-like, NGGM and MAGIC) using a closed-loop simulator based on the acceleration approach (Murböck, 2015; Schlaak & Pail, 2025).

The reference gravity-field variations resulting from mass redistributions within the hydrosphere (H), cryosphere (I), and solid Earth (S) are simulated using the HIS components of the ESA Earth System Model 2.0 (ESM2.0) (Dobslaw et al., 2015). In addition to the target signal, robust uncertainties are introduced to account for background models and instrumental errors. Aliasing errors arising from high-frequency mass variations in the atmosphere and ocean are modelled following Dobslaw et al., (2016). Tidal errors are estimated as the differences between the ocean tide models EOT11a (Savcenko et al., 2012) and GOT4.7 (Ray, 2008). Instrumental uncertainties are added to the line-of-sight (LOS) observations using product-specific noise models for the laser ranging interferometer (LRI) and accelerometers (ACC), including tone errors (Daras, 2026).

https://doi.org/10.5194/egusphere-2026-4642
Preprint. Discussion started: 7 August 2026

LOS observations, including the satellites position, velocity, and range rate, are then calculated for three different mission constellations. The GRACE-C-like satellite pair is simulated at an altitude of 493 km with an inclination of 89°, whereas NGGM is simulated at an altitude of 385 km and an inclination of 70°. The MAGIC constellation combines both satellite pairs. The Earth's gravity field is then recovered from the simulated LOS observations using different parameterisation strategies implemented by Schlaak & Pail, (2025). For NGGM simulations, spherical cap regularization is applied to mitigate polar gap effects (Pail et al. 2022, 2023; Metzler and Pail 2005; Heller-Kaikov et al. 2023).

The inversion yields Level-2a gravity-field products expressed as geopotential Stokes coefficients covering the 12-year period from 1995 to 2006, including 5-day and 30-day solutions resolved up to spherical harmonic degree and order 70 and 120, respectively. Level-2b products are generated using VADER filters (Horvath et al., 2018; Pail et al., 2022, 2023). The filtering scheme incorporates the expected signal variance and the formal variance–covariance matrix (VCM) obtained for each mission configuration (GRACE-C-like, NGGM, and MAGIC) and temporal resolution (5-day and 30-day) directly from the least-squares adjustment as the inverse of the normal-equation system.

Level-3 products are derived by transforming the geopotential Stokes coefficients into regularly gridded surface mass anomalies expressed as equivalent water height (EWH) using load Love numbers (Wahr et al., 1998). Prior to the transformation, the degree-0 and degree-1 coefficients have been replaced by the corresponding reference values from ESA ESM2.0. The C20 coefficient is replaced by SLR-like observations generated from ESA ESM2.0, with white noise introduced to represent SLR measurement uncertainties. The resulting gridded mass anomalies are corrected for glacial isostatic adjustment (GIA) using the trend component prescribed by ESA ESM2.0.

The resulting Level-2 and Level-3 products are used to assess the performance of the GRACE-C-like, NGGM, and MAGIC configurations for scientific and operational applications in hydrology, oceanography, glaciology, climate science, seismology, and geodesy.

3 Impact of NGGM and MAGIC on scientific applications and operational services

3.1 Hydrology

3.1.1 Drought monitoring

More than 1.8 billion people are currently affected by droughts, with 4.7% exposed to severe or extreme conditions; and under a 3°C warming scenario, an estimated 170 million people may regularly face extreme drought (UNCCD). Drought prediction and monitoring systems are being developed and implemented to mitigate the most serious consequences, for example,

https://doi.org/10.5194/egusphere-2026-4642
Preprint. Discussion started: 7 August 2026

agricultural losses affecting food, fibre, and fuel production and public-health challenges due to reduced water availability, reduced water quality, and amplified heat extreme. Only very few existing operational services—such as the European Drought Observatory (EDO; European Commission Joint Research Centre, s. d.-a) and the Global Drought Observatory (GDO; European Commission Joint Research Centre, s. d.-b)— include GRACE/-FO Total Water Storage Anomaly (TWSA) observations in their assessments, likely due to the limited spatial resolution of about 300 km and a latency of a few months. Satellite-derived soil moisture data come with low latency but can inform only the surface instead of accounting for deeper layers. It has been demonstrated that GRACE/-FO TWSA assimilation into hydrological models improves the spatial resolution compared to observations-only and at the same time vertically disaggregates TWSA into anomalies of compartmental storage, for example, groundwater and root zone soil moisture while improving the model realism. A system that already today integrates groundwater storage change from the GRACE/-FO-WaterGAP assimilation for drought risk assessments is the WWF risk filter (WWF, s. d.).

With respect to drought monitoring, we expect that with assimilating NGGM and MAGIC, we can derive more precise estimates of drought timing, drought duration, drought severity and drought prone area at low latency, and thus better initialize forecasts. Monitoring total water storage drought derived from assimilating NGGM and MAGIC data would exhibit lower uncertainties as compared to the use of GRACE-C-like mission data for assimilation. Here, we assimilate a synthetic truth augmented with simulated errors from the three mission scenarios GRACE-C-like, NGGM and MAGIC into the WaterGAP global hydrology model, similarly with settings close to the real GRACE/-FO WaterGAP assimilation (Gerdener et al., 2023). To identify drought events, we use the Drought Severity Index (DSI, Zhao et al., 2017) applied to total water storage anomalies (TWSA). The indicator follows a commonly used standardization technique, i.e. for each grid a climatology for the respective calendar month is removed and divided by the standard deviation of that month. The output of the indicator is classified into drought severity classes ranging from mild to exceptional drought. The methodological framework is described in more detail in Annex A.

https://doi.org/10.5194/egusphere-2026-4642
Preprint. Discussion started: 7 August 2026

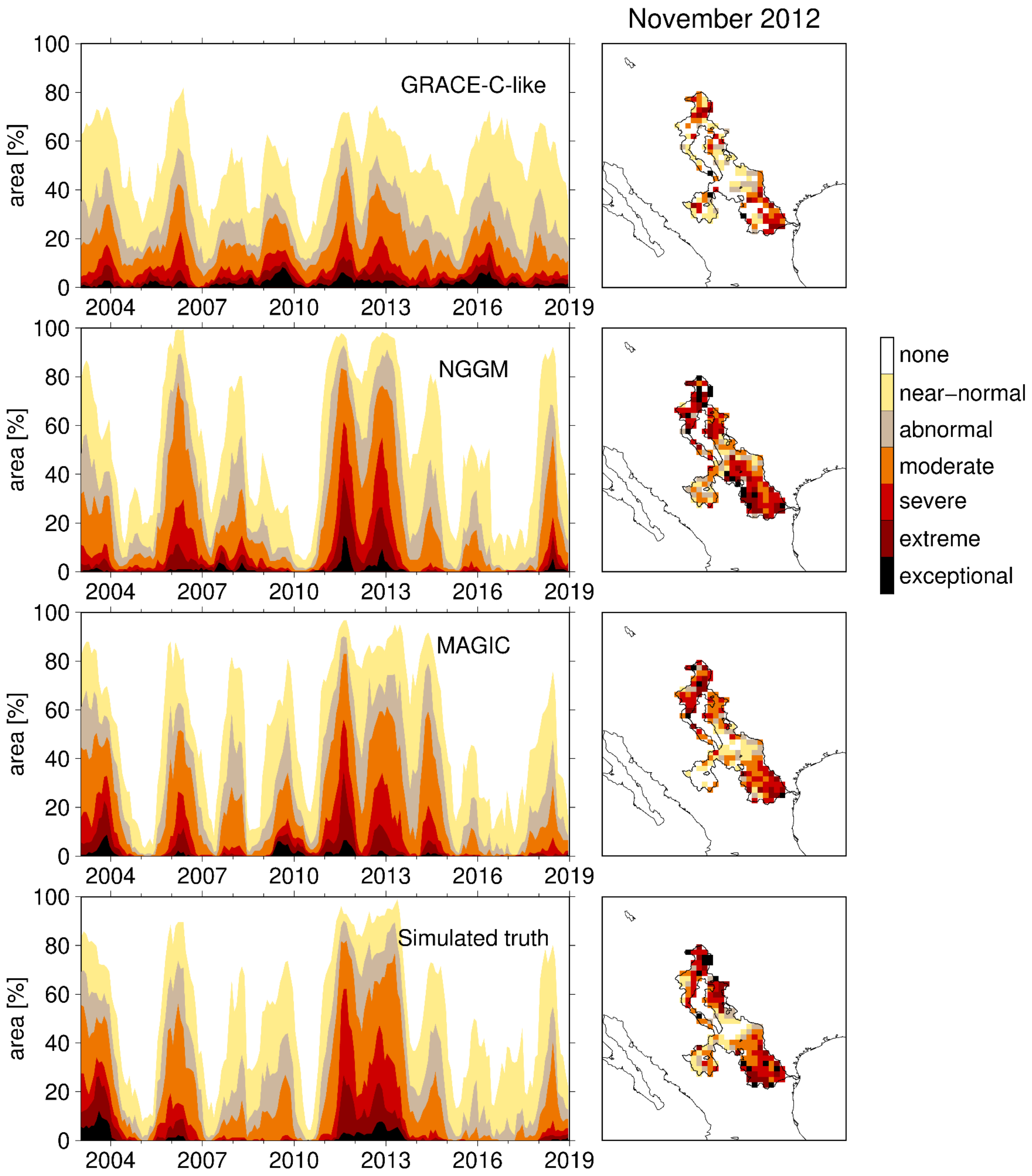

Figure 1: Percentage area of TWSA DSI severity classes for each month from 2003 to 2018 (left) and spatial maps for December 2012 (right) for using TWSA from GRACE-C-like (top), NGGM (middle top), and MAGIC (middle bottom) assimilation and from the simulated truth (bottom) for the Rio Grande River basin.

https://doi.org/10.5194/egusphere-2026-4642
Preprint. Discussion started: 7 August 2026

Figure 1 shows exemplarily the percentage area of the Rio Grande River basin that routes through the United States and Mexico, and which is affected by the different drought severity levels as identified from the TWSA-DSI for the three assimilations and the synthetic truth. The most dominant drought event that is found in the synthetic truth is observed in 2012 and 2013. With the NGGM- and MAGIC-assimilation, a larger area is identified as affected by severe to exceptional drought as compared to the assimilation with the GRACE-C-like mission. For the DSI in November 2012, severe or more intense drought is shown in the northern and southern parts of the Rio Grande River basin for the simulated truth, in contrast to the centre, where no drought is found in the truth. This pattern is also reflected in the DSI from NGGM and MAGIC assimilation, whereas the GRACE-C-like assimilation does not reflect this pattern as intensely. We look at the percentage drought agreement for the Rio Grande River basin, i.e. between the truth and the GRACE-C-like assimilation aggregated for all severity classes, 0.5° grids and months in 2003-2019. The agreement of GRACE-C-like-DA and the simulated truth is 57.02% for the Rio Grande River basin, while this increases up to 63.20% and 63.86 for the NGGM and MAGIC assimilation. This regional example can also be confirmed on a global scale: for about 86 and 95% of the 140 largest hydrological basins worldwide the drought agreement of NGGM and MAGIC assimilation with the simulated truth agrees better as compared to the GRACE-C-like assimilation, which highlights a strong benefit for monitoring the severity, timing and duration of a drought more precisely with the NGGM and MAGIC data assimilation systems.

We suggest that the use of NGGM and MAGIC observations in data assimilation frameworks would lead to enhancements in the spatial resolution and uninterrupted temporal coverage compared to standalone observations without assimilation, which is essential for operational services such as European Drought Observatory (EDO; European Commission Joint Research Centre, s. d.-a) and Global Drought Observatory (GDO; European Commission Joint Research Centre, s. d.-b). Furthermore, operational services could benefit from vertically disaggregated and temporally consistent water storage data sets such as, for example, deriving groundwater from assimilation for hydrological and agricultural drought monitoring. As the GRACE/-FO real world data assimilation is already nowadays integrated in drought monitoring and drought risk assessment tools, for example in the WWF Water Risk Filter, operational services and frameworks based on TWSA, groundwater, root-zone soil moisture and surface water would strongly benefit from NGGM and MAGIC assimilation to ensure updates of the products and improvements in spatial resolution. The integration of low-latency NGGM/MAGIC data with other hydrometeorological data and models is expected to further improve the capabilities of drought monitoring and drought risk assessment applications and services, in conjunction with an improved ability of monitoring deep soil water storage and groundwater resources. Society would benefit from these improved early warning systems, for example, by informing or predicting water shortages also in deeper layers of the soil required for plants and preventing the society from enormous harvest losses in irrigated areas.

3.1.2 Flood monitoring

Future gravity missions aim to increase the spatiotemporal resolution (e.g., 5 days) of TWSA retrievals and reduce uncertainty. Here, we investigated the added value of NGGM and MAGIC over a conventional GRACE-like mission (such as GRACE-C)

https://doi.org/10.5194/egusphere-2026-4642
Preprint. Discussion started: 7 August 2026

for high-resolution (0.1-degree and daily) hydrological DA, using W3RA as the baseline hydrological model. Based on L3 unfiltered TWSA 5-day data (2003–2006) from GRACE-C, NGGM, and MAGIC, we first developed a novel double-loop simulation–evaluation framework encompassing 180 DA scenarios across five DA resolutions, six filtering techniques, and two climatologically distinct basins (Brahmaputra and Danube). From this large sample we have shown the high sensitivity of DA to the configuration, and recommendation on the best configuration of each mission is given to maximize the potential of high-resolution NGGM and MAGIC data. The methodological framework is described in more details in Annex B.

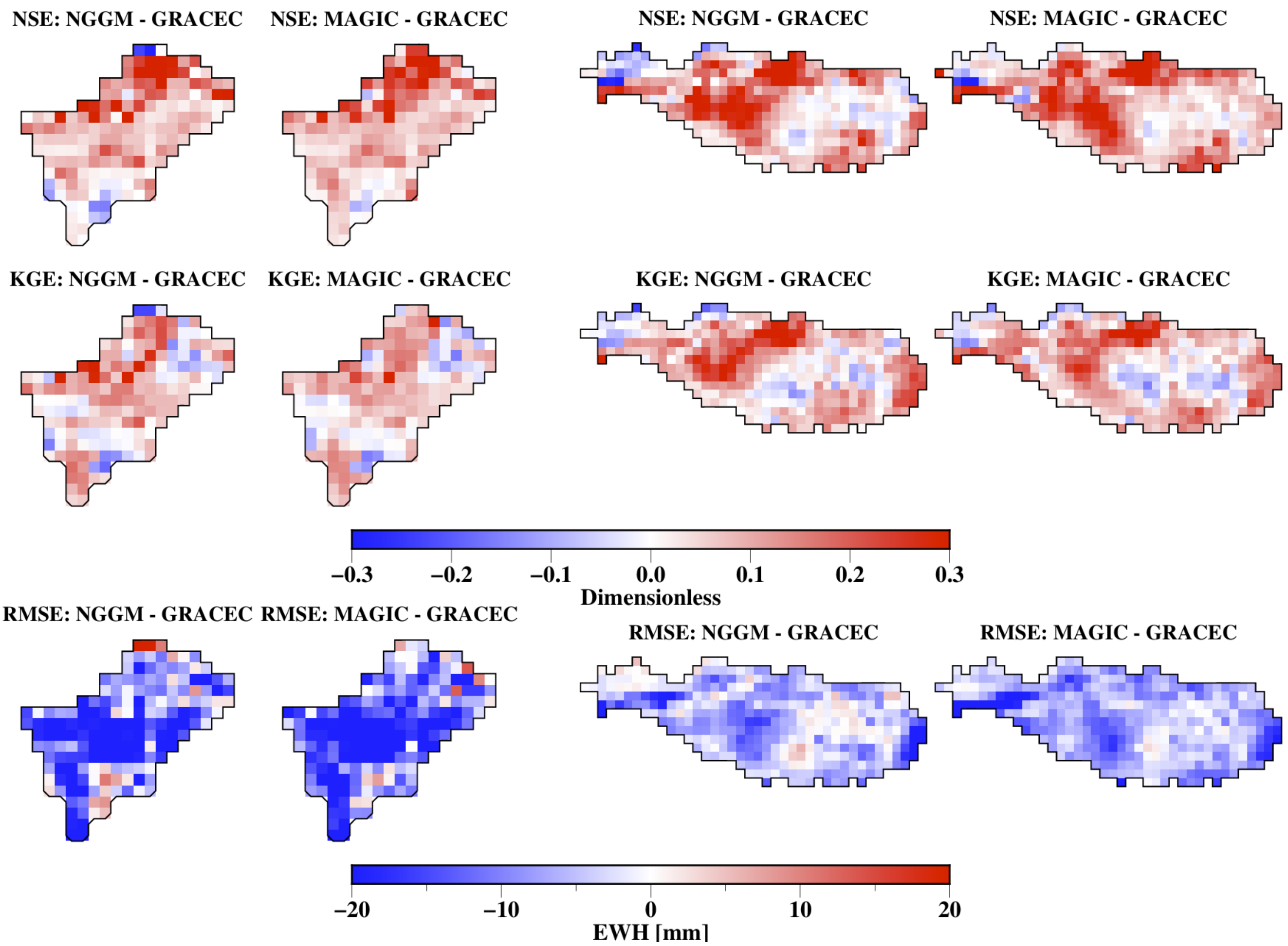

Figure 2: The added value of NGGM/MAGIC DA over GRACE-C DA, using the best DA scenario of each mission in terms of the NSE, KGE, and RMSE within the two study regions (Brahmaputra: the left two columns, and Danube: the right two columns). For NSE and KGE, the red indicates grid points where NGGM/MAGIC outperforms GRACE-C. For RMSE, the blue (negative) indicates grids where NGGM/MAGIC is better than GRACE-C.

https://doi.org/10.5194/egusphere-2026-4642
Preprint. Discussion started: 7 August 2026

Then, based on each's best DA configuration (see Figure 2), results indicate that MAGIC and NGGM perform comparably, both significantly outperforming GRACE-C by 21.8% (Brahmaputra) and 17.0% (Danube) in standardized KGE (Kling–Gupta Efficiency). The mean reduction in TWS Root Mean Squared Error (RMSE) is 13.6 mm (Brahmaputra) and 7.4 mm (Danube), corresponding to relative improvements of 37.8% and 60.2%, respectively. Spatially, the improvement of MAGIC/NGGM is dominating, see Figure 2. Last, through a synthetic flooding experiment, we confirm the capability of high-precision 5-day NGGM and MAGIC-DA to recover the fast-evolving hydrological signals, whereas GRACE-C is much less accurate to identify the temporal pattern of these signals. These findings demonstrate the substantial potential of NGGM and MAGIC for enhancing high-resolution hydrological DA to a level that is sufficient to realize flood monitoring and even prediction.

The results indicate that next-generation gravity missions such as NGGM and MAGIC have the potential to transform satellite gravimetry from a research tool focused on long-term water storage trends into an operational asset for water management and flood-risk assessment. By providing a ready-to-implement data assimilation framework, hydrological services could integrate high-precision, high-resolution Level-4 products immediately upon mission launch, reducing errors by 38–60% relative to current capabilities. The resulting performance gains would enable the detection of rapid water accumulation associated with flood events, exceeding the capabilities of existing gravity missions and providing actionable information on emerging flood hazards. Improved monitoring of water storage dynamics could enhance model initialization, strengthen large-scale flood forecasting and verification, and support flood-risk assessments in vulnerable river basins. More broadly, the findings highlight the potential of next-generation gravimetry to support water resource management and disaster preparedness during extreme events, further strengthening the societal value and operational relevance of such missions.

3.1.3 Precipitation monitoring

Accurate estimation of precipitation is essential for drought monitoring, water resources management, flood forecasting and water budget closure. Here, the SM2RAIN (Soil Moisture to Rainfall) algorithm (Brocca et al., 2015) is used to estimate precipitation from the inversion of the soil water balance equation forced with Level-3 5-day VADER filtered TWSA estimated for each mission configuration. The detailed description of SM2RAIN can be found in Annex C as well as in Brocca et al., (2015). The results in Figure 3 show the spatial distribution of simulated precipitation performance globally for GRACE-C-like, NGGM, and MAGIC compared to the ESM 2.0 during 2000-2006. The analysis is limited to grid cells where the annual precipitation is greater than 100 mm/year to focus on hydrologically active regions. Median R^2 increases from 0.31 (GRACE-C-like) to 0.37 (NGGM) and 0.38 (MAGIC), exhibiting improved representation of precipitation variability. The strong performance over central Africa and parts of South America are particularly noteworthy, as these regions are characterized by limited rain gauge coverage. This suggests that NGGM and MAGIC may enhance precipitation representation in observationally sparse regions, potentially reducing uncertainties associated with gauge-based products. Relative differences in R^2 confirm this behavior, with mean increases of +96.8% for NGGM and +100.6% for MAGIC. Improvements are most evident in mid- and high latitude regions, whereas humid tropical regions exhibit neutral or locally negative differences.

https://doi.org/10.5194/egusphere-2026-4642
Preprint. Discussion started: 7 August 2026

Overall, the ESM 2.0 configuration leads to better explained variance for both NGGM and MAGIC compared to GRACE-C-like. The results also open new opportunities to estimate precipitation for monitoring hydrological processes from terrestrial water storage (TWS) measurements, especially in data scarce regions.

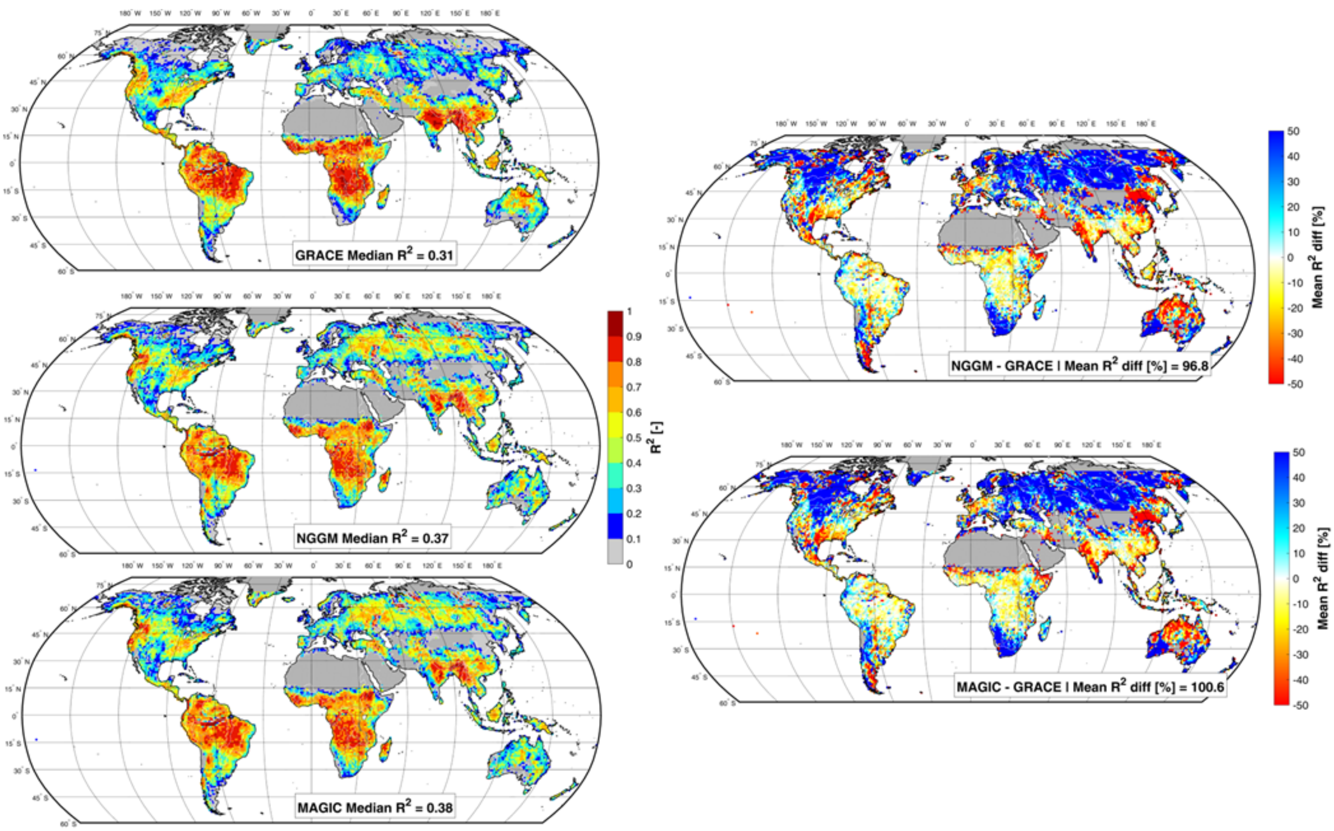

Figure 3: Spatial distribution of precipitation skill (R²) and relative performance differences (%) based on ESM 2.0 filtered configuration (NGGM, MAGIC and GRACE C-like), P > 100 mm/yr) globally for the period 2000-2006. Left panels show the coefficient of determination (R²) for GRACE-C-like (top), NGGM (middle), and MAGIC (bottom). The right panels present the relative difference in R² (%) between NGGM and GRACE (top) and MAGIC and GRACE (bottom).

High-resolution data from NGGM and MAGIC could be integrated into operational hydrological forecasting services, enabling more accurate predictions of floods and droughts. This is critical for disaster preparedness and water resource management. Specifically, gravimetry data could offer an alternative method of estimating precipitation, which is particularly important in areas without gauges, such as parts of Africa, south America and south-eastern Asia. In these regions, precipitation estimation using ground observations is less accurate, so satellite data can add value. NGGM and MAGIC can further improve the reliability and robustness of precipitation products used as input for flood forecasting and drought monitoring.

By providing precise and timely rainfall data, NGGM and MAGIC can help build climate resilience, support better agricultural practices (like optimizing irrigation), and aid in managing floods and droughts. This is especially helpful for regions with water shortages and can improve food security. The advancements from NGGM and MAGIC would allow for reliable precipitation estimation even in data scarce regions (e.g., mountainous areas, tropical forests), expanding the application of hydrological services worldwide.

3.1.4 Total Drainable Water Storage estimation

Total Drainable Water Storage (TDWS) represents the portion of terrestrial water storage that can naturally drain from a basin and contribute to runoff (Tourian et al., 2018). As such, it provides a valuable proxy for freshwater availability, highlighting the importance of its accurate quantification. Satellite gravimetry missions like GRACE/GRACE-FO measure changes in total water storage, but do not provide an absolute storage estimate or distinguish between drainable and non-drainable components. Therefore, TDWS has to be inferred indirectly, through the relationship between terrestrial water storage anomalies and runoff. This behavior is shown to follow a linear relationship for most of the large basins (Riegger & Tourian, 2014), which is used to estimate the drainable storage (Tourian et al., 2018). Details of estimation TDWS through R-S relationship is described in Annex D.

One key limitation in TDWS estimation comes from the effective spatial resolution of current gravity missions. This restricts robust TDWS estimation mainly to large river basins (e.g., Amazon: Tourian et al., 2018; Congo: Tourian et al., 2023; Mississippi: Ehalt Macedo et al., 2019). Here, we evaluate how future missions, such as NGGM and MAGIC, could improve the estimation of TDWS at the global scale, and potentially enable analyses at smaller basin scales. The improved spatial resolution from NGGM and MAGIC is expected to substantially alleviate these limitations by enhancing the separation of neighboring hydrological signals and reducing leakage from surrounding regions. Details of the datasets used in this study are provided in Table D1.

Figure 4 summarizes the TDWS estimation errors relative to ESM2.0 Ground Truth across 228 river basins covering a wide range of basin sizes. The global spatial distribution of TDWS derived from ESM2.0 ground truth is shown in Figure D1. The results demonstrate a clear improvement from GRACE-C to the next-generation mission scenarios. The median relative error decreases from 0.072 for GRACE-C to 0.040 for NGGM and 0.041 for MAGIC, corresponding to an overall improvement of approximately 40–45%. Similarly, the interquartile range (IQR), which reflects the spread of the error distribution, decreases from 0.180 for GRACE-C to approximately 0.091–0.092 for NGGM and MAGIC, corresponding to nearly a 50% reduction in variability.

https://doi.org/10.5194/egusphere-2026-4642
Preprint. Discussion started: 7 August 2026

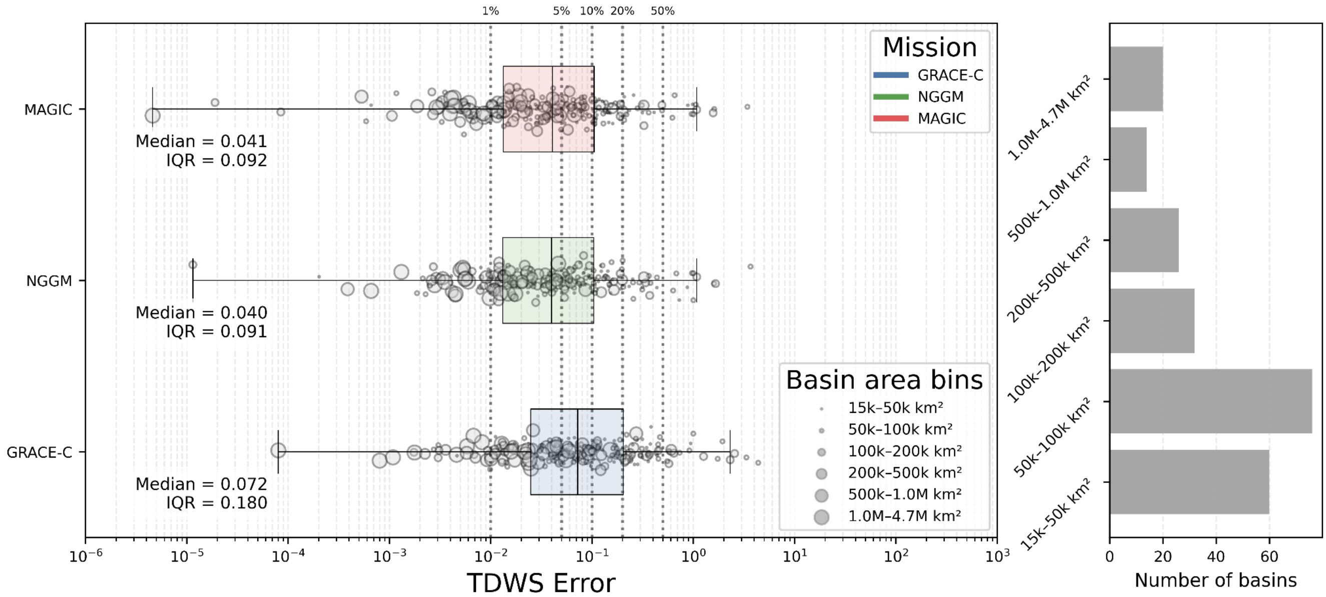

Figure 4 Distribution of TDWS relative estimation errors for GRACE-C, NGGM, and MAGIC across 228 river basins ranging from 15,000 km² to 4.7 million km². Circle size represents classes of basin area. Boxplots indicate the median and interquartile range of the relative errors for each mission scenario.

The narrower error distributions obtained for NGGM and MAGIC indicate not only lower overall uncertainty, but also more stable performance across a broad range of basin sizes. Nevertheless, smaller basins still exhibit relatively larger errors compared to large basins, reflecting the continued sensitivity of gravimetry-based estimates to spatial resolution and signal leakage at finer spatial scales. Despite these challenges, the next-generation missions significantly improve TDWS retrieval in small regions compared to the current GRACE-C capability. This enhanced performance opens the door to extending these analyses to smaller and more regional basins, thereby improving our ability to monitor global freshwater availability.

3.2 Ocean sciences

3.2.1 AMOC monitoring

Closed-loop simulations show that the future satellite gravimetry missions NGGM and MAGIC enable the recovery of midlatitude Atlantic Meridional Overturning Circulation (AMOC) variability at interannual and longer timescales with skill reaching up to 86 %, using western boundary ocean bottom pressure (OBP) alone. Compared to a GRACE-C-like configuration, the improved spatial resolution and reduced noise levels of NGGM and MAGIC substantially enhance sensitivity to low-frequency AMOC signals, allowing robust detection of circulation changes that are otherwise obscured. In particular, these missions permit the identification of AMOC trends of order 2 Sv per decade over periods as short as approximately 12 years and show sensitivity to rapid AMOC weakening or shutdown scenarios. This result establishes satellite

https://doi.org/10.5194/egusphere-2026-4642
Preprint. Discussion started: 7 August 2026

gravimetry as a viable, basin-scale observing system for monitoring large-scale ocean circulation variability and long-term change, complementary to existing in-situ measurements. The methodological framework used to complete these results is described in Annex E.

The ability of NGGM and MAGIC to provide continuous, basin-scale information on AMOC variability has clear relevance for operational ocean and climate services. Satellite-derived OBP indicators of overturning strength could be incorporated into operational reanalyses and monitoring frameworks, such as those supporting the Copernicus Marine Service, as an independent constraint on large-scale circulation variability. Unlike mooring arrays, which are geographically limited and operationally vulnerable, satellite gravimetry offers spatially coherent coverage that can reduce reliance on sparse in-situ observations. The improved detectability of trends and abrupt changes provided by NGGM and MAGIC supports the development of early-warning indicators of circulation change within climate services and enhances the robustness of long-range climate outlooks.

The Atlantic Meridional Overturning Circulation is widely recognised as one of the most consequential potential tipping elements in the Earth system, with a strong influence on North Atlantic climate, regional sea level, weather extremes, and large-scale rainfall patterns. A substantial weakening of the AMOC—whether gradual or abrupt—would have far-reaching societal consequences, including accelerated dynamic sea-level rise along the eastern seaboard of North America, disruption of European climate and storm tracks, shifts in tropical rainfall affecting food and water security, and reduced ocean heat uptake that could amplify global warming. Improving our ability to detect long-term AMOC trends and early-warning signals of destabilisation is therefore a societal priority. NGGM and MAGIC provide a unique opportunity to strengthen this capability by delivering sustained, meridionally-extensive observations of ocean bottom pressure that are dynamically linked to overturning variability. Beyond the risk of abrupt change, continuous monitoring of AMOC evolution also delivers substantial societal value by constraining slower circulation changes that influence decadal climate variability, coastal risk, and ecosystem dynamics. Robust, observation-based indicators of AMOC behaviour support climate adaptation planning, particularly for coastal infrastructure, flood-risk management, agriculture, and energy systems, and provide an independent benchmark against which climate-model projections can be evaluated. By enabling earlier and more reliable detection of circulation change, NGGM and MAGIC enhance climate situational awareness for policymakers, climate services, financial and insurance sectors, and international institutions, supporting evidence-based decision-making in the face of one of the most impactful and uncertain risks associated with long-term climate change.

https://doi.org/10.5194/egusphere-2026-4642
Preprint. Discussion started: 7 August 2026

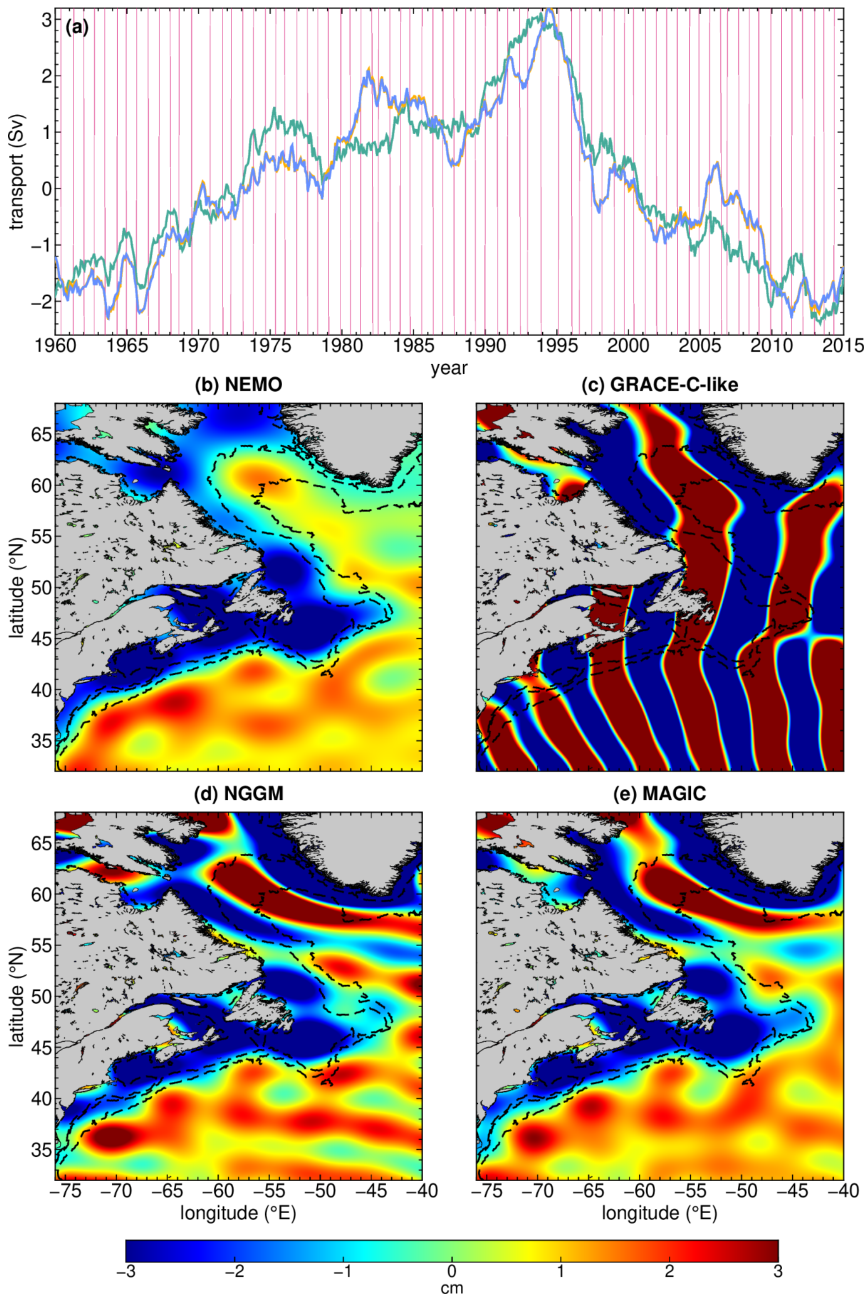

Figure 5 : AMOC recovery using geodetic ocean bottom pressure (OBP). (a) Target AMOC time series from NEMO (green), compared with AMOC reconstructions obtained from GRACE-C-like (red spikes), NGGM (blue) and MAGIC (yellow) mission simulations. Panels (b–e) show OBP anomalies for 1994, when the target AMOC reaches a maximum: (b) NEMO, (c) GRACE-C-like, (d) NGGM and (e) MAGIC. In all cases, OBP fields are truncated at spherical harmonic degree 70. Bathymetric contours are shown at 100 m, 1200 m and 3200 m. OBP is expressed in cm equivalent water height.

https://doi.org/10.5194/egusphere-2026-4642
Preprint. Discussion started: 7 August 2026

3.2.2 Sea level budget closure

Sea level integrates the response of multiple components of the climate system and therefore represents a key indicator of ongoing climate change. The oceans absorb about 90 % of the excess energy associated with the Earth's radiative imbalance, leading to thermal expansion, while land-ice mass loss provides an additional major contribution to global mean sea level rise (Forster et al., 2021; Fox-Kemper et al., 2021). The consistency between these processes and observed sea level change is commonly assessed using the Sea Level Budget (SLB) approach, which compares total sea level variations measured by satellite altimetry with the sum of steric changes derived from in-situ temperature and salinity observations and mass-driven changes observed by satellite gravimetry (Horwath et al., 2022).

Future satellite gravimetry missions such as NGGM and MAGIC are expected to substantially improve the observation of ocean mass redistribution through enhanced spatial resolution and reduced noise levels. Here, their potential contribution to SLB closure is assessed using simulated gravity solutions representative of GRACE-C, NGGM, and MAGIC mission configurations. Monthly fields of total sea level from satellite altimetry, thermosteric sea level derived from Argo observations, and manometric sea level from gravimetry are combined to estimate SLB residuals at both global and regional scales (see Appendix F).

The impact of each mission configuration is evaluated by comparing simulated gravimetric errors with observed SLB residuals. Regional error ratios quantify the fraction of the budget misclosure attributable to gravimetry errors, thereby providing a direct measure of how improved mission performance translates into enhanced budget closure across spatial and temporal scales. Diagnostics are analysed over periods ranging from 1 to 12 years using metrics based on linear trends, annual signal amplitudes, and interannual variability estimated from standard deviation (STD) of detrended and deseasoned time series. Further methodological details are provided in Appendix F.

Figure 6 presents the percentage of SLB residuals variability (STD) explained by simulated gravimetry errors for the different mission configurations. The comparison indicates a reduction of approximately 30 % in errors affecting the recovery of regional manometric sea-level variations at short and interannual time scales when using NGGM and MAGIC relative to a GRACE-C-like configuration, with the exception of the Arctic Ocean. NGGM notably improves SLB closure along the Antarctic Circumpolar Current, where error reductions locally reach up to 100 %, and also enhances budget consistency in the North Atlantic and major upwelling regions. MAGIC provides additional improvements over NGGM, particularly in polar regions where current gravimetric observations remain most challenging.

https://doi.org/10.5194/egusphere-2026-4642
Preprint. Discussion started: 7 August 2026

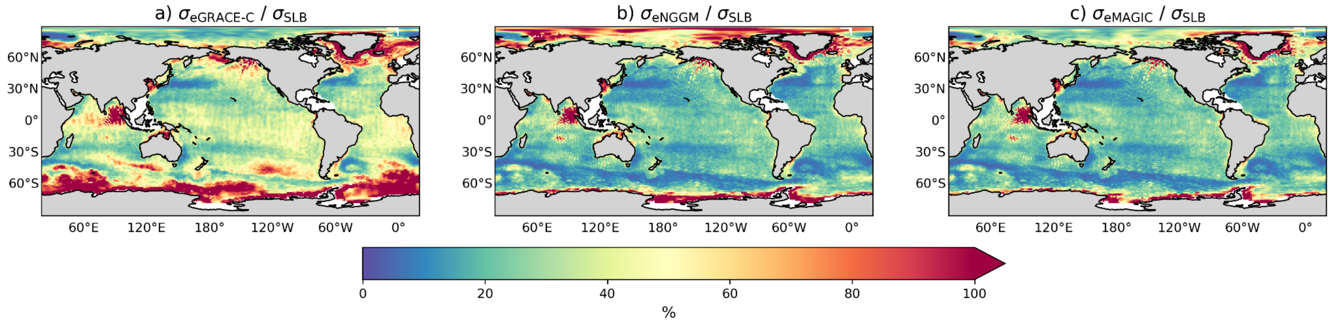

Figure 6 : Percentage of SLB residuals explained by the errors from gravity missions at high frequencies and interannual time scales (linear trend and annual signal removed) for GRACE-C (panel a), NGGM (panel b), MAGIC (panel c) simulations.

Consistent behaviour is observed across diagnostics. At the global mean scale, simulations indicate that gravimetry errors contribute only marginally to present-day SLB misclosure when realistic spatial filtering is applied, while NGGM and MAGIC exhibit reduced high-frequency variability compared to GRACE-C (supplementary material). Importantly, both next-generation configurations achieve error levels comparable to or lower than current SLB residuals even without strong filtering, highlighting their potential to reduce reliance on post-processing corrections required for present gravimetry missions. Complementary analyses performed at annual and decadal time scales further confirm the robustness of the improvements observed in Figure 6. While differences between mission configurations are less pronounced for linear trends and annual amplitudes, all metrics consistently indicate a reduction of gravimetry-driven errors from GRACE-C to NGGM and MAGIC, with the largest benefits emerging at short and interannual time scales. These additional results, including global mean diagnostics and regional evaluations based on trends and annual variability, are provided in supplementary material.

The Copernicus Marine Service provides free and open marine data to enable marine policy implementation, sustainable development of the ocean and scientific innovation. To achieve these objectives, the Copernicus Marine service provides high-quality oceanographic data and forecasts including sea surface temperature, currents, salinity, sea level, and biogeochemical parameters. At the moment, the Copernicus Marine Service does not distribute barystatic or manometric sea level data from satellite gravimetry, due to the large anisotropic errors in GRACE/-FO data and the relative novelty of the GRACE/-FO missions. The NGGM and MAGIC missions could contribute to the Copernicus Marine Service with the provision of robust estimation of the barystatic and manometric sea level changes enabling closure of the sea level budget, estimated concurrently to evaluate the quality of the ocean observation system. The range of potential users is broad, extending from climate scientists and operational oceanographers to policymakers, national climate agencies, and private stakeholders involved in insurance, coastal planning, and engineering.

https://doi.org/10.5194/egusphere-2026-4642
Preprint. Discussion started: 7 August 2026

The SLB closure exercise offers a powerful tool to better understand the drivers of sea level change and to assess the performance of the global observing system. SLB indicators can support climate assessments such as those of the IPCC by distinguishing the regional contributions to sea level change. In operational oceanography, accurate SLB data help validate general circulation models and improve their initialization. For policy and climate risk management, SLB indicators can inform national and regional adaptation strategies by distinguishing the regional contributions to sea level change and improve ocean model initialization for forecasting applications. SLB products can also serve educational and outreach purposes, as sea level is one of the most intuitive indicators of climate change and a crucial element in public communication.

3.3 Glaciology

Ice sheets are the largest potential source of future sea-level rise, yet projections of their contribution remain among the most uncertain components of global sea-level budgets (Aschwanden et al., 2021; Fox-Kemper et al., 2021; Fricker et al., 2025). A key source of that uncertainty is the poor observational constraint on extreme SMB events, both melt pulses in Greenland and anomalous snowfall episodes in Antarctica, which can temporarily dominate the annual mass budget and whose frequency and intensity are projected to increase under continued warming (Huai et al., 2025; Maclennan et al., 2025; Schnaubelt et al., 2025). By enabling accurate and timely detection of these events at basin scale, a dual-pair constellation such as MAGIC would substantially narrow the uncertainty band on ice-sheet mass-change reconstructions and projections. More precise attribution of short-term mass anomalies to their atmospheric drivers, combined with improved model validation, translates directly into more reliable sea-level rise projections on decadal timescales (Fettweis et al., 2020; Slangen et al., 2014). These projections underpin coastal flood-risk assessments, infrastructure planning, and climate-adaptation strategies in low-lying regions worldwide (Kopp et al., 2023; Oppenheimer et al., 2023). The capacity to detect and characterise extreme cryospheric events in near-real time would also strengthen early-warning systems and enhance the scientific basis for international climate policy, including assessments by the Intergovernmental Panel on Climate Change (Fox-Kemper et al., 2021; Oppenheimer et al., 2023). In this sense, the improvements demonstrated here for ice-sheet gravimetry contribute directly to the broader societal goal of reducing climate risk through improved Earth observation (Organization (WMO) et al., s. d.).

Within the ESA SING consortium, we evaluated how NGGM improves the detection of sub-monthly mass variability over Greenland and Antarctica as part of the MAGIC constellation. We used daily surface-mass balance (SMB) from the MAR regional climate model version 3.12 (Fettweis et al., 2017; Fettweis & Mattingly, 2023) for the signal estimate, while deriving noise levels from the ESA SING end-to-end gravity-field simulations (Section 2: Synthetic observations). We evaluated signal-to-noise ratios across drainage basins as a function of retrieval period, treated as a free parameter. This approach directly links mission performance and detectability to the timescales and spatial origin of melt and snowfall variability. The methodological framework is presented in Annex G, based on Sasgen et al. 2026.

https://doi.org/10.5194/egusphere-2026-4642
Preprint. Discussion started: 7 August 2026

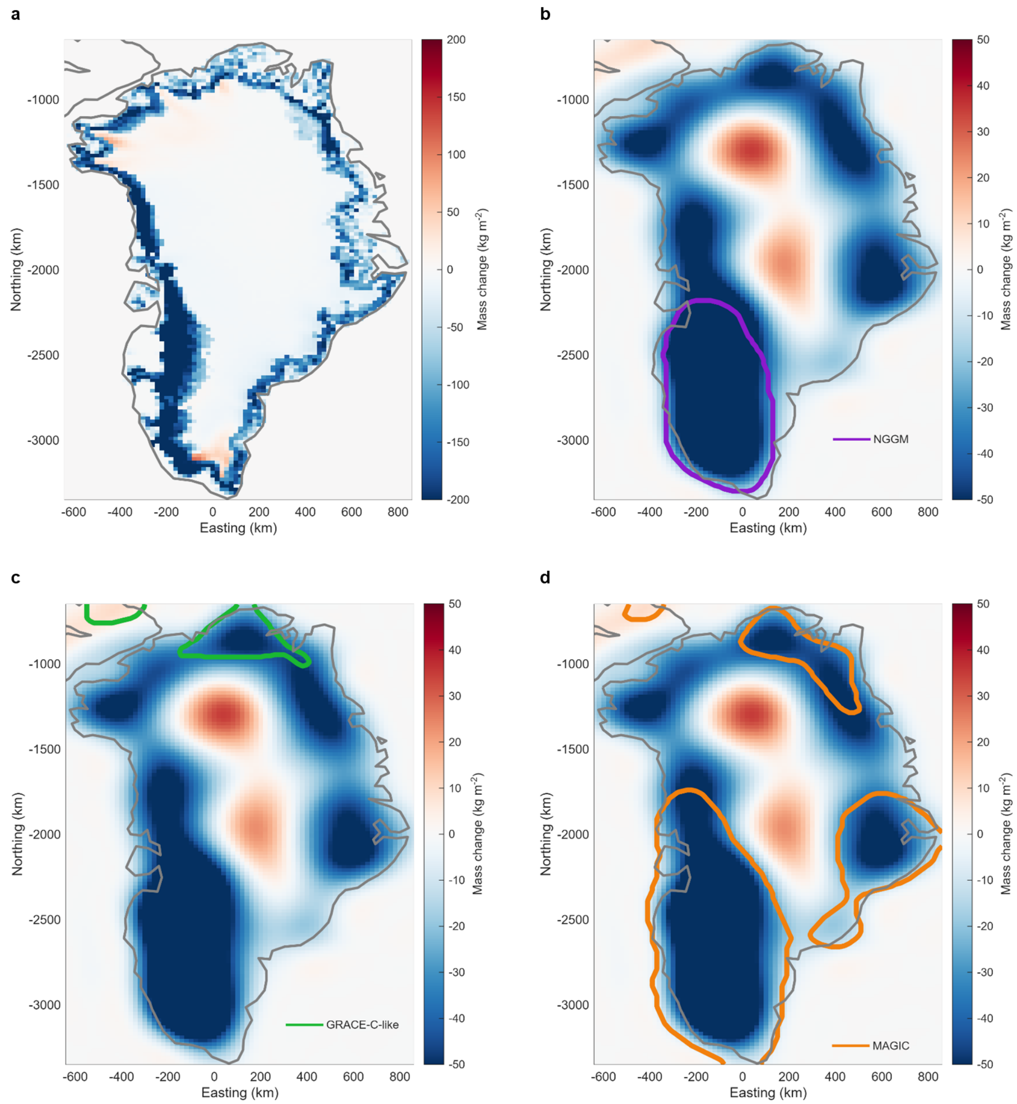

Figure 7 : Spatial mass change anomaly over Greenland during the peak of melt event in 2012. (a) Weekly surface-mass balance (SMB) anomaly at the modelled native resolution, (b-d) corresponding mass change anomaly represented up to cut-off degree 70. Contours indicate regions where the signal exceeds the noise threshold for a weekly retrieval period with mission scenarios (b) NGGM (purple), (c) GRACE-C-like (light green), and (d) MAGIC (orange).

For Greenland, MAGIC achieves weekly to bi-weekly detection limits across most drainage basins, with particularly strong performance along the southern and western margins where synoptic-scale melt events dominate short-term mass variability. Especially in these regions, NGGM enables detection of short-term variability that remains below the noise threshold of the single-pair, near-polar GRACE-C-like mission. This resolving power is sufficient to track the evolution of individual melt

https://doi.org/10.5194/egusphere-2026-4642
Preprint. Discussion started: 7 August 2026

episodes and to separate their contributions to basin-scale mass change, as demonstrated by the 2012 extreme melt case study with its double-peaked temporal structure (Figure 7). For Antarctica (not shown), where SMB variability is weaker and governed by intermittent storm-driven accumulation, MAGIC reaches bi-weekly resolving power in a subset of coastal basins along West Antarctica and parts of coastal East Antarctica, while the dry interior remains noise-dominated at sub-monthly scales. In particular, near-coastal improvements are driven by NGGM, whereas in both regions GRACE-C-like misses these short-lived signals. Especially for the ice sheets, MAGIC benefits from the mid-latitude and margin noise reduction provided by NGGM, while sustaining coverage over the entire ice sheets.

The sub-monthly resolving power demonstrated here represents a qualitative step change in what satellite gravimetry can offer to ice-sheet monitoring and modelling communities. Currently, the monthly temporal resolution, high noise floor and latency of GRACE/GRACE-FO preclude their use in near-real-time or operational monitoring of melt or snowfall extremes. MAGIC's weekly to bi-weekly retrieval capability facilitated by NGGM for key regions in the south of Greenland and along coastal East Antarctica, combined with its improved spatial resolution and the expected reduced processing latency, fundamentally changes this picture. Basin-scale mass anomalies from melt pulses or snowfall surges could be detected and attributed within days to weeks of their occurrence, enabling their assimilation into forecast models and SMB reanalysis. This opens a pathway toward operational gravimetry-based climate services for ice-sheet monitoring. In particular, the ability to resolve short-term SMB anomalies at basin scale would strengthen the validation and calibration of regional climate models such as MAR and RACMO, and support attribution of observed mass changes to specific atmospheric drivers (blocking highs, föhn events, atmospheric rivers), while improving understanding of meltwater retention and subsequent runoff processes. Such capabilities are currently unavailable, because monthly gravimetry products omit high-frequency temporal variability crucial for operational services of detection, attribution and prediction, especially of extremes.

3.4 Climate sciences

Anthropogenic greenhouse gas emissions have caused an energy imbalance (EEI) at the top of Earth's atmosphere, with the planet absorbing more energy than it emits. Measuring EEI is challenging due to its small variations relative to total energy fluxes, requiring high accuracy (≤0.3 W/m² per decade for long-term trends and ≤0.1 W/m² for monitoring). Since the ocean absorbs approximately 91% of excess energy, ocean heat content (OHC) serves as a crucial metric for assessing EEI (Meyssignac et al., 2019).

By integrating space altimetry and gravimetry measurements with in-situ data, the global OHC trend and mean EEI have been estimated at 0.75 W/m² [0.61, 1.04] (5–95% confidence level) (Marti et al., 2022). However, uncertainties—primarily driven by errors in GRACE and GRACE-FO data—must be reduced to meet the ≤0.1 W/m² accuracy required for effective monitoring. Tracking EEI variations is particularly challenging yet essential for evaluating climate change progression and the impact of greenhouse gas mitigation policies.

https://doi.org/10.5194/egusphere-2026-4642
Preprint. Discussion started: 7 August 2026

In this section we assess the influence of upcoming missions, including GRACE-C, NGGM, and MAGIC, on OHC and EEI error budgets across various temporal and spatial scales. The methodological framework developed to evaluate the added value of the NGGM and MAGIC missions relative to a GRACE-C–like scenario for EEI products is described in Annex H.

A key result of this study is the significant reduction in regional-scale OHC recovery errors achieved by NGGM relative to GRACE-C. Compared to a GRACE-C–like scenario, NGGM simulations exhibit substantially reduced errors, with reductions of up to 80% for OHC and 30% for OHU in the Southern Ocean (Figure 8). Similar results were obtained with MAGIC simulations (Not shown). Moreover, detailed results presented in Annex H show that the errors in GRACE-C-like simulations reach up to 20% of the expected OHC and OHU signals in regions such as the East South Pacific and exceed 50% at high latitudes and in the Indian Ocean. GRACE-C errors are consistent with uncertainty estimates derived from GRACE data. Finally, we evaluated the errors in EEI change estimates derived from manometric simulations. In terms of EEI, GRACE-C errors exceed those of NGGM and MAGIC by more than 30% in the mean (0.06 W/m²) and by 17% in the standard deviation (0.02 W/m²).

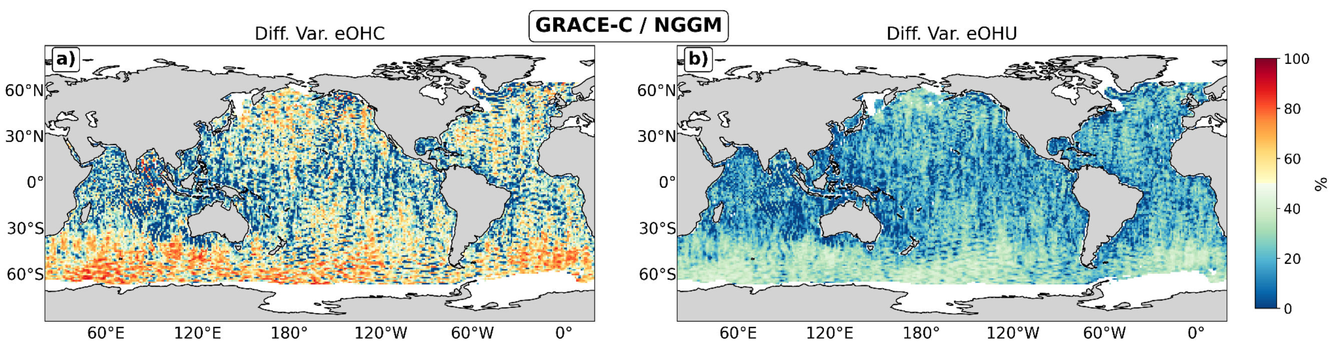

Figure 8 : Differences in the variance of OHC (a) and variance of OHU (b) errors between L3 GRACE-C and NGGM simulations. Percentage differences are relative to NGGM data.

The assessment of the upcoming gravimetry missions in terms of OHC and EEI error provides a robust framework to better understand the capability of the global observing system to monitor changes in the Earth's energy budget. Improving each component of the observing system is crucial for better tracking the EEI variations. It is essential for the early detection of the impacts of greenhouse gas mitigation efforts and for enhancing climate model accuracy, thereby supporting more informed long-term planning in sectors such as water resources, infrastructure resilience, and national security. OHC and OHU estimates derived from satellite gravity missions combined with auxiliary data, could be distributed by operational services such as the Copernicus Marine Service to be assimilated into global ocean reanalyses, incorporated into coupled weather and climate models, and applied in hazard monitoring systems.

https://doi.org/10.5194/egusphere-2026-4642
Preprint. Discussion started: 7 August 2026

3.5 Solid Earth Sciences

Documenting and modelling the deformation processes throughout the seismic cycle is a major objective of solid Earth sciences, as it improves our understanding of how stress accumulates and is released along major plate boundaries. This study assumes a layered viscoelastic Earth model consisting of an elastic lithosphere, a Burgers-type asthenosphere, and a Maxwell viscoelastic lower mantle (see Annex I). Analyses of GRACE and GRACE Follow-On data have shown the value of satellite gravimetry for investigating earthquake-related deformations from pre- to post-seismic phases through the corresponding mass redistributions (e.g. Chen et al., 2022 and references therein, Chao & Liau, 2019). Satellite gravity observations are sensitive to mass variations from surface to depth and a homogeneous spatial coverage on both sides of plate boundaries over land and ocean. Consequently, these datasets naturally complement seismological data and geodetic observations of surface displacements. Ground-based networks often lack coverage in remote and submarine regions, where many large ruptures may generate severe impacts, particularly in densely populated coastal areas.

Thanks to their improved resolution and accuracy, the NGGM and MAGIC missions will enable us to characterize co-seismic and post-seismic deformations for a larger number of lower-magnitude events than currently achievable using GRACE and GRACE Follow-On data. A first result is dedicated to the quantification of the co-seismic slip in terms of amplitude and orientation of the slip vector. One important aspect of NGGM and MAGIC is to determine whether the amount of co-seismic slip derived from the gravity signals could exceed that inferred from seismological data. Such a discrepancy would suggest the existence of rupture components outside the seismic frequency band, contributing to fault stress drop and surrounding stress redistribution.

For a Mw 8.5 thrust earthquake with a corresponding seismic moment of 7.16 × 1021 Nm, we generate synthetic co-seismic gravity signals using point-source modelling following Wang et al. (2017). The source geometry is defined by an east–west strike, a dip angle of 30°, and a rake angle of 30°, while the hypocentral location is set at 80 km depth and located at 110°E, 10°N. These parameters are assumed to be well constrained by seismological observations. This synthetic signal is added to NGGM, MAGIC or GRACE-C retrieval errors from a L2b, Vader filtered 5-daily simulation up to d/o 70, for the epoch of December 23, 2006 (see Supplementary Section S2.6). We then invert the obtained gravity observations for the along-dip and the along-strike components of dislocation, from which the slip orientation and amplitude factor respect to the synthetic reference can be deduced, and finally converted to seismic moment based on empirical relationships (Wells & Coppersmith, 1994) - as done when synthetizing the signal. We thus find that NGGM and MAGIC are able to retrieve the 30° slip orientation with ~5.58° of error, while the slip amplitude is retrieved with 9 % error (Figure 9). This corresponds to a factor of ~1.6 improvement with respect to GRACE-C, which is able to retrieve the slip orientation (resp. amplitude) with 8.77° (resp. 14 %) of error (Figure 9).

https://doi.org/10.5194/egusphere-2026-4642
Preprint. Discussion started: 7 August 2026

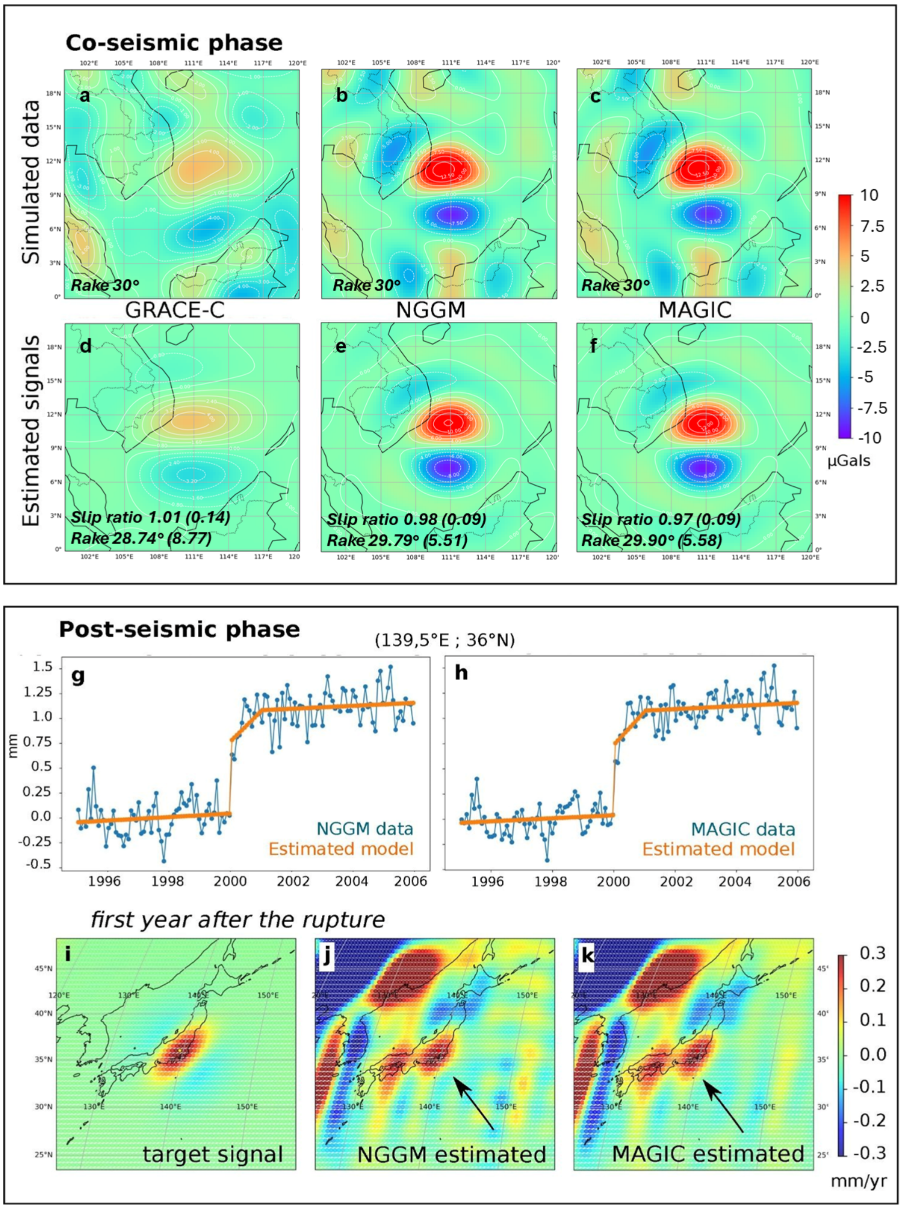

Figure 9 : Co-seismic slip inversion (Top panels) and early post-seismic trend estimation (Bottom panels) from GRACE-C, NGGM, and MAGIC. Panels a-c: synthetic 5-daily GRACE-C, NGGM and MAGIC gravity field observations. Panels d-f: gravity field changes from the estimated co-seismic models for each type of observation. The slip amplitude is described by its relative factor to the reference slip amplitude (slip ratio) ; the slip orientation is given by the rake angle (uncertainties in brackets). Panels g,h: time series of simulated NGGM and MAGIC data (blue) and estimated piece-wise linear model (orange). Panel i (resp. j, k): reference (resp. NGGM and MAGIC-estimated) post-seismic trend for the first year after the rupture. Data and results in panels g-k are all expressed as 500 km scale wavelet-transformed geoid variations.

A second result is dedicated to the quantification of early post-seismic relaxation signals. Here we take the example of a shallower Mw 8.5 thrust rupture, represented using a finite fault modelling (Wang et al., 2006). We consider 5 m of slip along the dip of a 450 x 80 km fault, with a 5 km top depth, 30° dip and a 220°N strike along the Japan subduction zone. In addition to the co-seismic gravity changes, we calculate five years of visco-elastic mantle relaxation after the rupture, considering a radially layered Earth with an elastic, 40 km thick lithosphere and a bi-viscous, 180 km thick asthenosphere (transient viscosity 5 1017 Pa.s, steady-state viscosity 1019 Pa.s), overlying the rest of the mantle (with 1020 Pa.s and 1021 Pa.s Maxwell viscosities in the 220-670 km depth range and below). This synthetic signal is added to a 1996-2006 time series of monthly NGGM, MAGIC and GRACE-C L2a geoid solutions up to d/o 100, assuming the earthquake takes place at the beginning of January 2000. At each location, we then estimate a co-seismic step, a short-term and a long-term post-seismic trend by least-squares fit of a piece-wise linear temporal model on the de-seasoned, wavelet-transformed time series. In this approach, the spatial wavelet transform acts as a local band-pass filter, facilitating the separation of the earthquake signals from the water cycle signals based on their different spatial scales and locations (Panet et al., 2007). We find that NGGM and MAGIC are able to retrieve the 0.33 mm/yr post-seismic rate of geoid variations during the first year after the rupture with errors of approximately ~8% and 4% respectively (Figure 9), whereas GRACE-C fails to resolve the signal due to striping artefacts. The retrieved post-seismic signals provide valuable constraints to document the short-term deformation processes following large earthquakes, and improve constraints on the viscosity structure of the asthenosphere.

By improving the co-seismic slip models and documenting the short-term post-seismic deformation processes, particularly through quantifying the contributions of aseismic creep and visco-elastic relaxation of the lower crust and the mantle after a rupture, NGGM and MAGIC will improve the models of stress redistribution along nearby faults following an earthquake, and thus better assess the risk of failure of other faults after a major seismic event. At the same time, these observations will improve constraints on the geographical extent and severity of earthquake events. All these results are expected to improve seismic hazard assessment in the vicinity of major plate boundaries. In addition, the NGGM and MAGIC co-seismic and post-seismic gravity signals, expressed in equivalent water heights, can be used to correct and improve water storage estimates in seismically active regions.

3.6 Geodesy

To assess the NGGM and MAGIC impact on geodesy, the focus was twofold, referring both to modeling the temporal variations of potential values at core sites of the International Height Reference Frame (IHRF) and quantifying the effect on precise orbit determination (POD). As far as the IHRF is concerned, the available 12-year simulated L2b dataset was employed to estimate variations of gravity potential (ΔW), as well as geoid height, physical height, and ellipsoidal height variations and their trends at selected IHRF stations. The NGGM and MAGIC impact was assessed against ESM2.0, which was used as a reference. In the frame of POD, the NGGM and MAGIC impact was investigated within the context of precise orbit determination, which offers a sensitive validation tool for an in-orbit assessment of a given gravity field model. The POD

https://doi.org/10.5194/egusphere-2026-4642
Preprint. Discussion started: 7 August 2026

study used the unfiltered L2a simulated data and examined POD and inter-satellite K-Band Ranging (KBR) analysis for GRACE and POD and inter-satellite Laser Ranging Interferometry (LRI) analysis for GRACE-FO, respectively. The methodological framework is presented in detail in Annex J.

In terms of the impact to the IHRF, NGGM performance was found to be better than GRACE-C for 22%-52% and MAGIC better than GRACE-C for 44%-57%, referring to the examined IHRF stations (12 stations spanning the entire globe). At higher latitudes (> ~55o), the improvement for NGGM dropped to ~11-13% and that of MAGIC to ~15-18%. In the investigation of GRACE KBR range-rate residuals, NGGM provided improved results by 39.5% and MAGIC by 39.6%, compared to GRACE-C, while for GRACE-FO LRI range residuals, the improvement reached 77.3% for NGGM and 77.6% for MAGIC. Finally, for GRACE-FO LRI range-rate residuals, NGGM was superior by 64.2% and MAGIC by 64 % compared to GRACE-C.

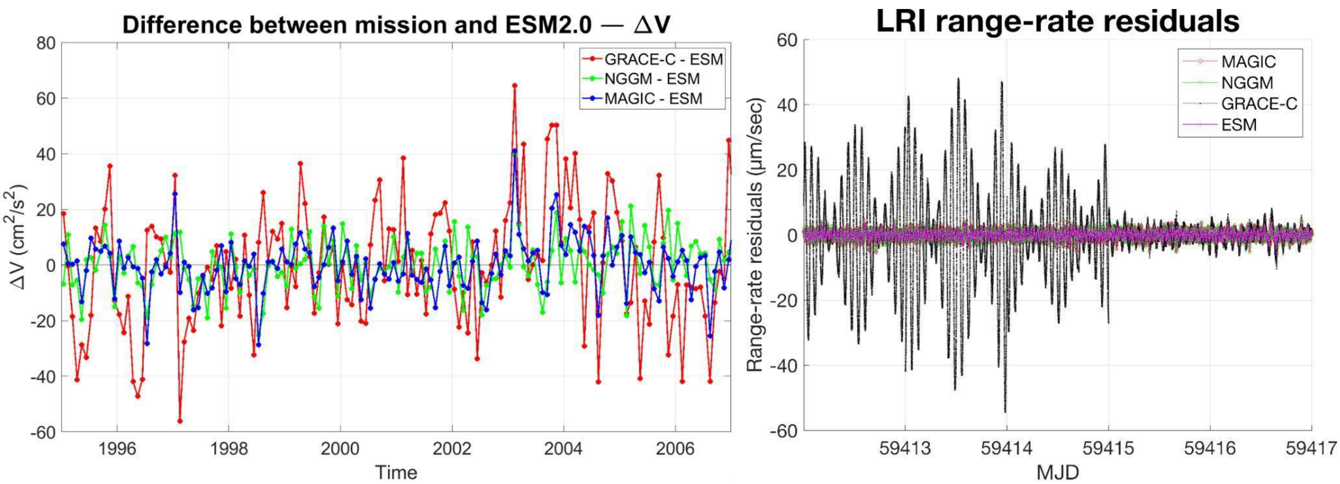

Figure 10: Potential differences to ESM2.0 from GRACE-C, NGGM and MAGIC at the AUT1 IHRF station (left). GRACE-FO LRI range residuals using the GRACE-C, NGGM and MAGIC gravity models (right).

The NGGM and MAGIC products can be integrated to operational services such as the IHRF Coordination Center of the International Association of Geodesy, which is responsible for delivering potential values for the IHRF sites as well as the local vertical datum offsets to the conventional Wo value of the IHRF. In terms of POD, the NGGM and MAGIC 5-day and monthly gravity models can contribute to improved POD of earth observation satellites, e.g., the recent Sentinel 6 altimetry mission, where highly accurate POD is needed in the pursuit of a mm- to cm-level sea surface height determination.

The societal benefit of the mission results will be seen in POD for Low Earth Orbiters (LEOs) data processing, especially in LEO Positioning, Navigation and Timing (PNT), which is a topic that requires highly accurate orbits in (near-) real time for positioning purposes. NGGM and MAGIC missions will also be advantageous to the unification of Vertical Reference Frames

https://doi.org/10.5194/egusphere-2026-4642
Preprint. Discussion started: 7 August 2026

(VRFs) and Height System Unification (HSU), the realization of the International Height Reference System (IHRS) into the IHRF, the determination of potential value rates for the IHRF stations, in accordance with the International Terrestrial Reference Frame (ITRF) and conventional GNSS levelling, thus contributing to many engineering sectors, promoting sustainability, safety, and economic growth.

4 Main scientific advances expected from NGGM and MAGIC

The ESA SING project provides a comprehensive end-to-end assessment of the performance of the NGGM and MAGIC missions for monitoring key Earth's system variables across hydrology, oceanography, glaciology, climate science, solid Earth sciences, and geodesy. Using a closed-loop simulation framework with robust estimation of instrumental, tidal, and aliasing uncertainties, the ESA SING project quantifies the added value delivered by NGGM and MAGIC relative to GRACE-C-like missions across a broad range of high-level Earth system products.

In hydrology, NGGM and MAGIC assimilation scenarios substantially improve the estimation of terrestrial water storage anomalies (TWSA) and the assessment of derived hydrological variables, particularly at high spatial and temporal resolution. The NGGM and MAGIC assimilation scenarios based on a global hydrological model improve the representation of drought timing, severity, and spatial extent relative to the GRACE-C–like assimilation. Drought characteristics are more accurately recovered across most river basins worldwide, with significant gains in the representation of extreme events and in data-sparse regions. In high-resolution hydrological models, assimilation of fast-track NGGM and MAGIC products substantially enhances TWSA reconstruction skill compared with GRACE-C–like missions, with KGE improvements of up to ~22% and RMSE reductions of up to ~60%, resulting in a more faithful representation of rapid hydrological variability relevant to flood monitoring and forecasting. When used to force a simplified hydrological model, NGGM- and MAGIC-derived TWSA improve the representation of precipitation variability, particularly in humid tropical regions with sparse in situ observations, thereby enhancing the reliability of precipitation products used for flood forecasting and drought monitoring in remote and data-sparse regions. Both missions improve the accuracy and spatial resolution of Total Drainable Water Storage (TDWS) estimates while reducing leakage errors, lowering relative errors by ~40–45% and extending robust basin-scale monitoring to a broader range of smaller river basins, thereby strengthening regional freshwater availability assessments.

In oceanography, NGGM and MAGIC enhance Ocean Bottom Pressure (OBP) observations through improved spatial and temporal resolution, reduced noise, and longer temporal coverage, leading to more accurate estimates of the mass component of ocean circulation and sea-level variability. Closed-loop simulations show that both missions recover interannual and decadal AMOC variability from ocean bottom pressure with higher skill (up to ~86%) and greater sensitivity to low-frequency signals than GRACE-C–like missions. Robust detection of AMOC trends (~2 Sv per decade over ~12 years) and improved sensitivity to pluriannual-to-pluridecadal weakening or shutdown scenarios establish satellite gravimetry as a basin-scale observing system complementary to in situ measurements. Relative to GRACE-C–like missions, NGGM and MAGIC improve sea-level

https://doi.org/10.5194/egusphere-2026-4642
Preprint. Discussion started: 7 August 2026

budget closure by reducing gravimetry-driven errors, particularly at local scales and for high-frequency to interannual variability, with the largest gains occurring in regions strongly affected by atmosphere–ocean aliasing, including the Southern Ocean, North Pacific, North Atlantic, and Equatorial Atlantic. NGGM drives most improvements in accuracy and resolution, while MAGIC extends polar coverage and temporal sampling.

In glaciology, the largest gains are achieved with the MAGIC double-pair configuration, which enables detection of smaller and faster ice-mass changes through improved spatiotemporal resolution and reduced errors. MAGIC supports weekly to bi-weekly monitoring of ice-mass anomalies across Greenland and parts of Antarctica, substantially improving detection of short-lived melt and snowfall events relative to GRACE-C–like missions. At mid-latitudes, NGGM alone improves detection of sub-monthly mass variability, particularly along coastal margins, but lacks coverage poleward of ~72° latitude, limiting its use in highest-latitude polar regions.

In climate sciences, synthetic gravity observations generated within the ESA SING project were used to assess the closure of the energy budget at global and regional scale scales. Historical gravimetry, altimetry, and Argo data yield global mean ocean heat uptake (GOHU) accuracy of 0.2–0.3 W/m^2 (2003-2015). With VADER-filtered simulations, GRACE-C-like missions contribute up to 0.19 W/m^2 uncertainty, while NGGM and MAGIC improve this by 30–40%, achieving ~0.12–0.13 W/m^2 accuracy. NGGM and MAGIC also enhance the stability and temporal consistency of GOHU retrievals. Regionally, NGGM and MAGIC outperform GRACE-C by up to 80% in recovering ocean heat content changes at mid-latitudes (30–60° N/S). NGGM and MAGIC recover mean and temporal variations in ocean heat uptake at regional scales with up to 50% higher accuracy than GRACE-C.

In Solid Earth sciences, NGGM and MAGIC will extend observations of co-seismic and post-seismic deformation to a much larger number of lower-magnitude earthquakes than currently detectable with GRACE, GRACE-FO, and GRACE-C–type missions. Improved constraints on co-seismic slip, aseismic fault creep, and viscoelastic relaxation will enhance understanding of earthquake-cycle processes and support more accurate assessments of stress transfer, fault reactivation, and seismic hazard.

In geodesy, NGGM and MAGIC will directly improve observations of the time-variable gravity field, leading to more accurate estimates of gravity potential, geoid change, and height-system evolution at IHRF sites. Relative to GRACE-C-like missions, improvements are estimated at ~22–52% for NGGM and ~44–57% for MAGIC. In precise orbit determination, inter-satellite ranging residuals are reduced by up to ~40% for KBR and ~77% for LRI observations, strengthening global height reference frame realization and gravity-field-based orbit determination.

https://doi.org/10.5194/egusphere-2026-4642
Preprint. Discussion started: 7 August 2026

5 Outlook for operational services

Higher spatial and temporal resolution, improved accuracy, reduced latency, and extended temporal coverage provided by the NGGM and MAGIC missions have the potential to transition satellite gravimetry from a research-oriented capability toward a component of operational Earth observation infrastructure.

5.1 Integration into operational monitoring and forecasting services

Several high-level Earth observation products derived from NGGM and MAGIC gravity data through data assimilation and data fusion frameworks could be integrated directly into existing environmental monitoring and forecasting services.

Improved monitoring of terrestrial water storage and its partitioning into surface water, soil moisture, especially in the root zone, and groundwater will strengthen operational products within the Copernicus Climate Change Service (C3S) and Copernicus Global Land Service (CGLS). These enhanced Level-4 hydrological datasets will support a wide range of downstream applications, including drought and flood monitoring, water resources assessment, groundwater management, irrigation planning, reservoir operations, and climate services. By providing more accurate and timely information on total and subsurface water availability, they will improve early-warning indicators and forecasting capabilities in systems such as the European Drought Observatory (EDO), Global Drought Observatory (GDO), Global Flood Awareness System (GloFAS), and Famine Early Warning Systems Network (FEWS NET), particularly for drought risk assessment, freshwater availability monitoring, and agricultural water management.

NGGM and MAGIC-derived products such as ocean bottom pressure (OBP), barystatic and manometric sea level changes, ocean heat uptake (OHU), Earth Energy Imbalance (EEI), and Atlantic Meridional Overturning Circulation (AMOC) indicators can be delivered directly to operational services such as the Copernicus Marine Service or AVISO. These data products can then be used to improve the forcing, calibration, and evaluation of ocean reanalyses and forecasting systems, as well as coupled ocean–atmosphere prediction systems used for climate monitoring and forecasting.

NGGM and MAGIC-derived products will provide higher-resolution and higher-frequency estimates of glacier and ice-sheet mass balance, enabling the detection of short-term melt and accumulation events as well as longer-term trends. This improved temporal and spatial sampling can support operational cryosphere and climate services such as the Copernicus Climate Change Service (C3S), the National Snow and Ice Data Center (NSIDC), and the WMO Global Cryosphere Watch (GCW), which require consistent mass-change information for monitoring and downstream products.

5.2 Climate monitoring and early detection of climate tipping points

The NGGM and MAGIC missions will strengthen the observation of several Essential Climate Variables (ECVs) defined by the Global Climate Observing System (GCOS), including terrestrial water storage, soil moisture, groundwater, glaciers and ice sheets, sea level, and ocean heat content. Improved accuracy, resolution, and continuity of these observations will provide a stronger observational basis for quantifying climate change and evaluating the Earth system response to greenhouse gas forcing.

Enhanced ECVs records will improve the detection and attribution of long-term climate trends and provide critical constraints for early-warning indicators of abrupt climate system tipping points. Improved monitoring of ocean bottom pressure and sea-level variability will strengthen the detection of long-term AMOC changes and provide more robust observational constraints on its stability and potential approach toward a critical transition. More accurate observations of ice-sheet mass balance will improve the detection of accelerated mass loss and provide stronger observational constraints on the potential destabilization of the Greenland and Antarctic ice sheets. Improved estimates of ocean heat uptake will enable more accurate monitoring of the Earth's Energy Imbalance, a fundamental metric of climate change that responds to greenhouse gas forcing decades before corresponding changes become fully apparent in global mean surface temperature.

Consequently, the advanced data products generated by NGGM and MAGIC will directly support international climate governance and global monitoring frameworks. The reduction of uncertainties in land-ice mass balance and ocean heat uptake improves the accuracy of climate assessments and global stocktake reporting coordinated by the Intergovernmental Panel on Climate Change (IPCC), the World Climate Research Programme (WCRP), and the United Nations Framework Convention on Climate Change (UNFCCC). Furthermore, the high-resolution ice-sheet and glacier mass change products will actively constrain intercomparison initiatives and regional monitoring services operated by the Ice Sheet Mass Balance Intercomparison Exercise (IMBIE), the Glacier Mass Balance Intercomparison Exercise (GlaMBIE), the Copernicus Climate Change Service (C3S), the National Snow and Ice Data Center (NSIDC), the WMO Global Cryosphere Watch (GCW), the Scientific Committee on Antarctic Research (SCAR), and the International Arctic Science Committee (IASC).

5.3 Natural Disaster Response & Mitigation

NGGM and MAGIC have the potential to substantially strengthen natural disaster monitoring, forecasting, and risk assessment through improved observations of hydrological extremes, tectonic processes, and sea-level change.

In hydrology, the enhanced spatial and temporal resolution and reduced latency of terrestrial water storage data will improve their assimilation into hydrological models, enabling more accurate monitoring and forecasting of floods and a better characterization of rapid water accumulation associated with extreme events. These advances can support earlier and more reliable flood warnings, improved disaster preparedness, and more effective management of water-related hazards.

In solid Earth sciences, the missions will enable the detection of gravity signals associated with large earthquakes ($M_w \geq 8$), including both seismic and aseismic

https://doi.org/10.5194/egusphere-2026-4642
Preprint. Discussion started: 7 August 2026

deformation. Combined with seismic and geodetic observations, these measurements will improve the characterization of earthquake rupture processes, post-seismic deformation, and stress redistribution, thereby supporting hazard assessment, damage mapping, and the evaluation of cascading seismic risks.

For coastal hazards, improved observations of the mass component of sea-level change will provide more accurate estimates of regional and coastal sea-level rise. These products will support coastal risk assessments, adaptation planning, resilient infrastructure design, and the management of coastal ecosystems and freshwater resources.

Together, these capabilities demonstrate the potential of NGGM and MAGIC to extend satellite gravimetry from a climate-monitoring tool to a key component of future disaster-risk reduction and resilience frameworks.

5.4 Geodetic infrastructure and satellite operations

NGGM and MAGIC will improve geodetic infrastructure by providing more accurate and temporally resolved gravity field models, benefiting precise orbit determination (POD), orbit prediction, and low-Earth-orbit satellite navigation. The enhanced gravity information is expected to improve the accuracy of real-time and near-real-time orbit determination, with particular relevance for positioning, navigation, timing applications, and space-debris tracking. In geodesy, the missions will strengthen the realization of the International Height Reference Frame (IHRF) and support the unification of regional vertical reference systems through improved geoid models and estimates of their temporal evolution. These advances will enable more accurate GNSS-based height determination and improve the monitoring of vertical land motion, sea-level change, and geophysical hazards. The resulting geodetic products will support large-scale engineering projects, disaster risk assessment, coastal management, and urban planning, particularly in regions affected by sea-level rise, subsidence, and other forms of ground deformation.

Appendix A: Drought monitoring and prediction

Assimilation setup

Three assimilation scenarios are used to perform the evaluation on drought monitoring: the GRACE-C-like, NGGM, and MAGIC assimilation scenarios. The three scenarios are set up using a real-GRACE/-Fo assimilation scenario (Gerdener et al., 2023), where monthly total water storage anomalies (TWSA) from gravity observation are assimilated into a global hydrological model, the WaterGAP model operating at about 50 km spatial resolution (Mueller Schmied et al., 2024). In order to perform the assimilation experiments, two different model versions will be used:

1. A model that serves as input observation into the data assimilation system. This serves as the simulated truth

https://doi.org/10.5194/egusphere-2026-4642
Preprint. Discussion started: 7 August 2026

2. A different model setup will be used for the model that is underlying the assimilation system

Compared to model 1, model 2 has systematic errors included. The simulated observational input for the assimilation is then perturbed on a monthly basis by using the empirical error information of the GRACE-C, NGGM and MAGIC scenarios. Both the perturbed simulations and the variance-covariance matrices are used as input to the data assimilation system. We here use a VADER-filtered variance-covariance matrix provided by TU Munich. For the perturbation of the simulated truth, we use a full variance-covariance matrix. Following common practice, error correlations are reduced for the assimilation to enable a stable output. The assimilation is performed here using the Ensemble Kalman Filter (EnKF, Evensen, 2003) and the Parallel Data Assimilation Framework (PDAF, Nerger et al., 2020), an open source environment for data assimilation that contains filter algorithms and tuning strategies. Finally, for this analysis, we extract the monthly TWSA derived from the simulated truth and the GRACE-C-like-, NGGM, and MAGIC-assimilation scenarios for the monitoring of drought.

Drought monitoring

To derive monitored drought events from time series is by using drought indicators. A common TWSA drought indicator is the Drought Severity Index (DSI, Zhao et al., 2017) . This indicator uses a simple standardization technique applied to the TWSA. For each grid cell, the indicator computes a climatology for a specific calendar month j, for example, January, and the corresponding standard deviation for that month. As next, the current indicator value of month j and year i is derived by removing the climatology from the current water storage in month j and year i and divide it by the standard deviation via

$$DSI_{i,j} = \frac{x_{i,j} - \bar{x}_j}{\sigma_j} \quad \text{(A1)}$$

The resulting index values are classified into severity classes ranging from -2.0 (exceptional drought) to +2.0 (exceptionally wet) as shown in Table A1. Under the assumption that the storage is Gaussian distributed, the lowest severity class of exceptional drought would mean that 2.1% of the months are exceptionally dry.

Table A1: Drought severity classes of the DSI as described in Zhao et al. (2017).

	Drought Severity Index [-]	
Drought classes	**Minimum**	**Maximum**
Abnormal	-0.8	-0.5
Moderate	-1.3	-0.8
Severe	-1.6	-1.3
Extreme	-2.0	-1.6

https://doi.org/10.5194/egusphere-2026-4642
Preprint. Discussion started: 7 August 2026

Exceptional		-2.0

Appendix B: Flood monitoring and prediction

Data assimilation setup

Although the `truth (ESM2)' and `model (W3RA)' are fixed, the DA (data assimilation) results vary depending on the choice and configuration of the assimilated satellite gravity data. To identify optimal DA configurations and maximize each satellite mission, six strengths of spatial filtering are tested by changing the regularization factor of the Kuala-based regularization filtering. In addition, the DA is implemented at five different spatial resolutions, where TWS estimates were introduced into the model in grids of 1-degree, 2-degree, 3-degree, 4-degree or in terms of basin average.

Two climatologically different study regions were selected to further diversify the DA setup: (1) the Brahmaputra and (2) the Danube River basins. The signal-to-noise ratios (SNR) of satellite-based TWS are very different in these basins. The standard deviation of the basin-average signal (synthesized from the truth) is found to be 165.5 mm, while the standard deviation of the corresponding noise (i.e. residuals from the truth) is 41.7 mm (GRACE-C), 17.4 mm (NGGM) and 12.3 mm (MAGIC); for Danube, the signal is 59.4 mm, while the corresponding noise is 29.3 mm (GRACE-C), 17.7 mm (NGGM) and 13.0 mm (MAGIC). This means that for two study regions and three satellite gravity missions, 180 variants of the DA scenarios are performed (180 = 2 basins * 3 missions * 6 filtering choices * 5 resolution choices). This large sample enables us to identify the optimized DA setup for each satellite mission, and also confirms the importance of regional tuning of DA since the SNR of each study region can differ dramatically.

In addition, the impact of error representation of each mission on the DA is addressed. While the noise of satellite missions can be well reduced by the dedicated filtering, the signal is inevitably smoothed and leaks to the neighbour due to the convolution nature of the filtering. This type of signal loss is widely known as damping error or leakage bias. However, the eventual propagated covariance in previous DA setup can only account for the noise rather than the signal damping error. Therefore, in this study, in addition to the nominal 'propagated covariance', we also consider the case of a realistic covariance that incorporates the damping error, whereas this is only doable in the simulation studies. These new realistic covariances are used to perform another set of DA experiments in Brahmaputra and Danube for each satellite mission to understand the added value of NGGM/MAGIC over GRACE-C in the 'best case'.

Conceptual experiment for flood monitoring

Flood monitoring DA experiment is further performed based on the previous experience, i.e., the optimized DA setup over Brahamaputra. The L2b filtered gravity data and empirical variance-covariance matrix (VCM) is used for the DA at 1-degree

https://doi.org/10.5194/egusphere-2026-4642
Preprint. Discussion started: 7 August 2026

resolution (which was identified as the best setup) in this experiment. Subsequently, it is essential to generate a synthetic truth encompassing the flooding signal. In this step, W3RA is adopted to generate the individual compartment (surface runoff, soil moisture, groundwater, snow and biomass) and the total (total water storage, TWS). For simplification one year (2005) is selected for experiment, where ERA5 forcing field is adopted to drive the W3RA model. To synthesise the 'flooding signal', we adjusted the magnitude of the precipitation over specific days in summer of 2005. Then, each gravity mission adds its 'measurement noise' to the synthetic truth to further generate the 'observations'. In this way, data assimilation driven by our PyGLDA toolbox is performed for each scenario and for each gravity mission. It is worth mentioning that in the DA the forcing field is not perturbed, which means that the model cannot reproduce the 'flooding' event' but the observations (by gravity mission) can. Evaluation is carried out to see how much 'flooding' signal can be captured by the DA.

Appendix C: Precipitation monitoring

Input Data for Precipitation Estimation

In this study, the SM2RAIN algorithm (Brocca et al., 2014) was applied to total water storage (TWS) data derived from the ESA Earth System Model (ESM 2.0) to estimate precipitation. First, the algorithm was driven by the "true" TWS simulated by ESM2.0 to derive a corresponding "true" precipitation dataset. The ERA-Interim precipitation used to force the ESM2.0 simulations served as the reference for evaluating the capability of SM2RAIN to retrieve precipitation from TWS observations. This step was necessary because SM2RAIN has traditionally been applied to surface soil moisture observations rather than terrestrial water storage represented by TWS. Subsequently, synthetic experiments were performed by applying the same methodology to the filtered TWS products generated for the GRACE-C-, NGGM-, and MAGIC-like mission configurations. The resulting precipitation estimates were then compared with the reference precipitation to assess the performance and added value of the future gravity mission scenarios.

Methodology for Precipitation Estimation

A modified version of the SM2RAIN algorithm, i.e., using TWS instead of soil moisture, was applied to estimate precipitation between two successive TWS measurements in the time interval dt, by inverting soil water balance equation as follows:

$$Z^* \frac{dTWS^*(t)}{dt} = p(t) - r(t) - e(t) - g(t) \tag{C1}$$

Here Z* [mm] represents the water capacity of the soil layer, calculated as the product between the depth of the soil layer and its porosity. The term TWS* refers to the relative TWS [–] (i.e., ranging between 0 and 1); t is the time, p is the precipitation rate [mm t−1], r(t) is the surface runoff rate [mm t−1], e(t) is the evaporation rate [mm t−1] and g(t) is the drainage rate [mm t−1]. During precipitation events, evaporation and surface runoff are assumed to be negligible (Brocca et al., 2015). The drainage rate is dependent on TWS, which is derived from Famiglietti and Wood's (Famiglietti and Wood, 1994). Thus, the precipitation rate can be estimated by simplifying Eq. (2) as follows:

https://doi.org/10.5194/egusphere-2026-4642
Preprint. Discussion started: 7 August 2026

$$p(t) = Z^* \frac{dTWS^*(t)}{dt} + as(t)^b \quad \text{(C2)}$$

Where a (mm t −1) and b (–) refer to the saturated hydraulic conductivity and the exponent in the (Famiglietti and Wood, 1994) equation, respectively. Calibration is performed independently at each grid cell (point-by-point) using a gradient-based optimization function. The procedure estimates five parameters: Z*, a, b, Tpot, and Tbase. The estimation of parameters a, b, and Z* is needed to compute the precipitation between two consecutive TWS* measurements. The filter parameters (T_pot and T_base) have narrow interquartile ranges, indicating consistent noise reduction across grid cells. Before running the algorithm, the noise in the TWS signal is reduced by applying the exponential filter as described by Brocca et al. (2019), where the characteristic time length parameter (T) is modeled as a function of soil moisture using a two-parameter power law relationship. The values of the two parameters (T_pot and T_base) of the modified exponential filter equation, and the a, b, and Z* parameter values are estimated through calibration against the ERA Interim (ERAI) precipitation dataset. The calibration is carried out by minimizing an objective function based on the Nash–Sutcliffe efficiency (NS, Nash and Sutcliffe, 1970), computed between simulated and reference precipitation (e.g., ERAI).

Appendix D: Total Drainable Water Storage estimation

Input Data

Table D1 summarizes the datasets used in this study. We use Level-3b (L3b) gridded TWSA products simulated for three satellite gravity mission scenarios: GRACE-C–like mission, NGGM, and MAGIC. These simulations are based on the ESA Earth System Model: ESM2.0, covering the period 1995–2006. The synthetic gravity observations are provided at 30-day temporal resolution, and VADER-filtering is applied. A further requirement for TDWS estimation is to derive the storage–runoff relationship. We use GloFAS (Van Der Knijff et al., 2010) to derive the storage–runoff relationship.

Table D1: Datasets used for the estimation of TDWS

Dataset/Model	Variable(s)	Resolution
GloFAS	Discharge, Snow Water Equivalent	0.05°, daily
Simulated gravity observations (for MAGIC, NGGM, and GRACE-C-like missions)	TWSA (L3b, VADER-filtered)	1°, 30-day
ESM2.0	TWSA (Ground truth)	1°, 30-day
GRDC watershed boundaries	Basin mask	Global

https://doi.org/10.5194/egusphere-2026-4642
Preprint. Discussion started: 7 August 2026

Estimation of TDWS

The estimation of TDWS follows the runoff--storage framework introduced by Tourian et al., 2018, which links basin-scale river discharge to satellite-derived TWSA. Runoff, expressed as the river discharge observed at the basin outlet and divided by the contributing basin area, is assumed to vary linearly with the drainable portion of total basin storage:

$$Q(t) = \frac{1}{\tau}\left(S_O + \Delta S_{\phi}^{d}(t)\right) \quad \text{(D1)}$$

where $Q(t)$ is runoff, $\Delta S_{\phi}^{d}(t)$ denotes the phase-corrected drainable water storage anomaly (DWSA), τ is the hydraulic time constant, and S_O is the storage offset, which corresponds to TDWS. The DWSA is derived from TWSA by excluding storage variations such as snow, lake, wetland, and reservoir storage, that are not consistently involved in runoff generation, as:

$$\Delta S^{d}(t) = \Delta S(t) - \sum_i \Delta S_i^{nd}(t) \quad \text{(D2)}$$

where $\Delta S(t)$ represents TWSA and $\Delta S_i^{nd}(t)$ denotes the anomaly of the i-th non-drainable storage component.

Another aspect of the runoff--storage relationship is the temporal lag between changes in basin storage and the corresponding runoff response. This lag can introduce hysteresis into the runoff--storage relationship and weaken its linear behavior. Therefore, correcting for the storage-runoff lag is the next step for restoring a near-linear relationship and obtaining a robust estimate of TDWS.

$$\Delta S_{\phi}^{d}(t) = \Delta S^{d}(t + \Delta t) \quad \text{(D3)}$$

where Δt denotes the time lag. The resulting $\Delta S_{\phi}^{d}(t)$ represents the DWSA after alignment with the observed runoff response. The lag between runoff and storage can be corrected by using a frequency-dependent phase-shift correction (Tourian et al., 2023). After applying the non-drainable storage correction and the phase-shift correction, TDWS is estimated by fitting the linear runoff--storage relationship to the paired runoff and DWSA time series (See Figure D1).

Mission TDWS Performance Evaluation

All simulated mission datasets, including GRACE-C, NGGM, and MAGIC, are processed using the same TDWS workflow. Because the processing strategy is identical across all missions, differences in the resulting TDWS-related parameters can be attributed to mission design rather than algorithmic differences. The ESM2.0 is used as the reference truth, allowing us to assess how closely each mission reproduces basin-scale hydrological behavior. For each basin and mission scenario, TDWS-related parameters are estimated and compared with the corresponding ESM2.0-derived reference parameters. The accuracy of each mission is evaluated using error metrics as illustrated in Figure D1. For TDWS, the normalized error is defined as

$$\Delta S_O = \frac{\left|S_0^{(m)} - S_0^{(ref)}\right|}{S_0^{(ref)}} \quad \text{(D4)}$$

where $S_0^{(m)}$ is the mission-derived TDWS estimate and $S_0^{(ref)}$ is the ESM2.0 reference TDWS. This metric expresses the deviation from the reference TDWS in dimensionless form, enabling direct comparison among missions and basins.

https://doi.org/10.5194/egusphere-2026-4642
Preprint. Discussion started: 7 August 2026

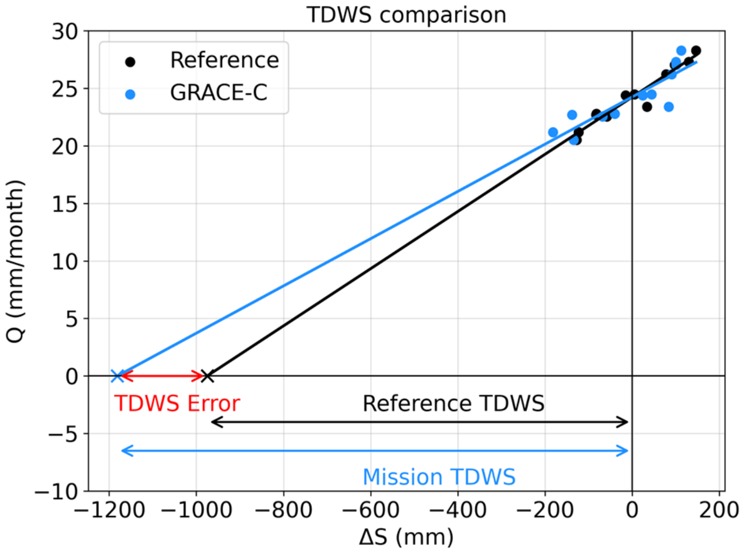

Figure D1: Illustration of the TDWS error

Appendix E: AMOC monitoring

The ESM2 simulations used for the satellite-gravity observing-system experiments did not include dynamically evolving ocean variability. We therefore added an ocean-dynamic signal derived from monthly mean output from a free-running, non-assimilating configuration of NEMO, designated ORCA0083-N06, run at the UK National Oceanography Centre, Southampton. The model is configured on a tripolar grid with a nominal horizontal resolution of 1/12° and 75 vertical levels. Following an initial adjustment from World Ocean Atlas 2005 initial conditions, the model is forced using the DRAKKAR Forcing Set version 5.2, DFS5.2 (Brodeau et al., 2010; Dussin et al., 2014). Prior to 1979, DFS5.2 is based on the ERA-40 reanalysis from the European Centre for Medium-Range Weather Forecasts. From 1979 onward, ERA-40 is blended into fields from ERA-Interim, which provides improved spatial and temporal resolution (Dee et al., 2011). The forcing dataset supplies the surface atmospheric variables required by the NEMO bulk formulae to compute air–sea fluxes of heat, freshwater and momentum, including 10-m wind components, 2-m air temperature and humidity, downward short- and long-wave radiation at the sea surface, and total and solid precipitation. Further details of this model configuration are given by Marzocchi et al. (2015).

Ocean bottom pressure (OBP) in NEMO was expressed as equivalent water height and computed as the difference between sea surface height and steric height:

$$p(\theta,\lambda,t) = h(\theta,\lambda,t) - s(\theta,\lambda,t) \tag{E1}$$

https://doi.org/10.5194/egusphere-2026-4642
Preprint. Discussion started: 7 August 2026

where h is sea surface height relative to the geoid, s is steric height, θ is latitude, λ is longitude, and t is time. Global means were removed from both quantities prior to forming the difference. Steric height was computed as:

$$s(\theta, \lambda, t) = -\int_{-H}^{0} \frac{\rho(\theta,\lambda,t) - \rho_0}{\rho_0} dz \tag{E2}$$

where ρ is seawater density computed from the model potential temperature and salinity fields, $\rho_0$is a reference seawater density, $H(\theta, \lambda)$ is the local water-column depth, and z is depth. The integral was evaluated numerically on the model's discrete vertical grid.

To combine the NEMO OBP fields with the Level-2 Stokes coefficients from the mission simulations, the monthly OBP fields on the native distorted NEMO grid were first interpolated to a regular 1/12° global latitude–longitude grid using quadrilateral bilinear interpolation. The gridded OBP fields were then expanded into fully normalised spherical-harmonic coefficients. For degree l and order m, the cosine and sine coefficients were computed as:

$$\Delta C_{lm}(t) = \frac{3\rho_w}{4\pi\rho_E R_E} \frac{1+k'_l}{2l+1} \int_\Omega p(\theta,\lambda,t) \underline{P}_{lm}(cos\theta) cos(m\lambda) d\Omega \tag{E3}$$

$$\Delta S_{lm}(t) = \frac{3\rho_w}{4\pi\rho_E R_E} \frac{1+k'_l}{2l+1} \int_\Omega p(\theta,\lambda,t) \underline{P}_{lm}(cos\theta) sin(m\lambda) d\Omega \tag{E4}$$

where ΔC_{lm} and ΔS_{lm} are the cosine and sine Stokes coefficients, ρ_w is the density of freshwater, ρ_E and R_E are the mean density and radius of the Earth, k'_l is the degree-dependent load Love number, $\underline{P}_{lm}$ are fully normalised associated Legendre functions, and dΩ is the element of solid angle. The expansion was computed to degree and order 120.

The simulated mission products provide a shorter 12-year time series of Level-2 Stokes-coefficient errors as compared to the 1958–2015 NEMO record. To construct a 58-year combined record, the mission-simulation coefficients were first detrended. The resulting anomaly sequence was then repeated forward and backward in time, with alternating forward and reversed copies, until the full NEMO period was spanned. These repeated mission coefficients were added to the NEMO Stokes coefficients to produce synthetic observations containing both the NEMO ocean-dynamic signal and mission-specific observing-system errors.

For each mission simulation and each truncation degree N = 1, …, 120, gridded OBP fields were reconstructed from the combined Stokes coefficients as:

$$p_N(\theta,\lambda,t) = \frac{\rho_E R_E}{3\rho_w} \sum_{l=1}^{N} \left\{ \frac{2l+1}{1+k'_l} \sum_{m=0}^{l} \underline{P}_{lm}(cos\,\theta) [\Delta C_{lm}(t)\, cos(m\lambda) + \Delta S_{lm}(t)\, sin(m\lambda)] \right\} \tag{E5}$$

https://doi.org/10.5194/egusphere-2026-4642
Preprint. Discussion started: 7 August 2026

The reconstructed fields were evaluated on a regular 1/12° grid over the North Atlantic. From these fields, area-mean OBP time series were computed over two regions on the western boundary slope: an upper-slope region between the 100 and 1200 m isobaths, denoted $U_N(t)$, and a lower-slope region between the 1200 and 3200 m isobaths, denoted $L_N(t)$. The AMOC transport estimate was then computed from the cross-slope OBP contrast:

$$\widehat{M}_N(t) = 2[L_N(t) - U_N(t)]/3 \tag{E6}$$

The unit conversion factors and mid-latitude geostrophic parameters are such that OBP expressed in cm of equivalent water height gives transport in Sverdrups. The factor 2/3 accounts for the approximate difference in depth range represented by the lower- and upper-slope regions, with the lower-slope depth interval spanning roughly twice the upper-slope interval.

The target AMOC time series was diagnosed directly from the NEMO velocity fields. Zonal transports were computed along arcs of constant latitude at half-degree intervals between 35°S and 65°N. Arcs were used rather than straight zonal sections because the tripolar model grid becomes increasingly distorted toward high northern latitudes. At each latitude and depth, the zonally integrated transport was obtained by summing the meridional velocity and the northward-facing component of the zonal velocity along the latitude arc. The overturning streamfunction was then computed by vertically integrating the zonally integrated transport. For each latitude and monthly time step, the maximum value of the overturning streamfunction was taken to represent the AMOC strength at that latitude. A representative basin-scale AMOC time series, $M(t)$, was then obtained by averaging this latitude-dependent AMOC strength over the subtropical North Atlantic, 16–46°N.

The ability of each simulated mission to recover the known NEMO AMOC variability was assessed as a function of truncation degree using a skill score. Prior to comparison, both the target AMOC time series and the satellite-derived estimate were filtered to isolate the timescale of interest. Skill was then defined as:

$$\delta_N = 1 - \frac{\Sigma_t[\widehat{M}_N(t) - M(t)]^2}{\Sigma_t M(t)^2} \tag{E7}$$

where $M(t)$ is the filtered NEMO AMOC target and $\widehat{M}_N(t)$ is the corresponding filtered AMOC estimate recovered from the truncated satellite-gravity OBP fields. A skill of one indicates perfect recovery of the target time series, a skill of zero indicates performance equivalent to predicting zero anomaly at all times, and negative values indicate poorer performance than this reference prediction.

https://doi.org/10.5194/egusphere-2026-4642
Preprint. Discussion started: 7 August 2026

Appendix F: Sea level budget closure

Input Datasets and Components

The sea level budget is decomposed into three primary observed components, each derived from distinct geodetic and oceanographic sources:

Absolute Sea Level (ΔSL_{abs})

Regional and global absolute sea level changes are observed via satellite altimetry. The primary source is the Copernicus Climate Change Service (C3S) multi-mission product (version DT2021), providing $1/4^{\circ}\times1/4^{\circ}$ daily grids. This dataset integrates data from reference missions (TOPEX/Poseidon, Jason-1/2/3, and Sentinel-6) and is corrected for specific instrumental drifts, including the TOPEX-A altimeter drift and the Jason-3 microwave radiometer wet tropospheric correction.

Manometric Sea Level (ΔSL_{man})

The manometric (or mass-related) component is derived from satellite gravimetry (GRACE and GRACE-FO). Two main products are utilized: the AVISO+ ensemble (incorporating 60 spherical harmonic solutions to capture processing uncertainties) and the GFZ GRAVIS post-processed solutions. These data are corrected for Geocenter motion (C10,C11,S11), Glacial Isostatic Adjustment (GIA), and have specific low-degree coefficients (C20,C30) replaced by Satellite Laser Ranging (SLR) estimates for improved accuracy.

Steric Sea Level (ΔSL_{steric})

The steric component, accounting for changes in ocean density due to temperature (thermosteric) and salinity (halosteric), is estimated using in-situ Argo profiles. Gridded interpolated fields (such as ISAS20 from Ifremer) are used to compute sea level changes down to 2000 m depth. Calculations follow the Thermodynamic Equation of Seawater 2010 (TEOS-10) standards. The deep ocean contribution (>2000 m) is typically treated as a small constant or addressed through specific deep-Argo estimates.

Vertical Land Motion (ΔVLM)

Vertical Land Motion (VLM) represents the changes in the height of the seafloor relative to the reference ellipsoid, acting as the necessary link between geocentric (absolute) sea level and the physical seafloor. The primary contributor to this component is Glacial Isostatic Adjustment (GIA), which describes the long-term viscoelastic response of the Earth to past deglaciation. This study utilizes GIA corrections derived from Spada & Melini (2019), to account for both seafloor deformation and geoid changes. Furthermore, the VLM component incorporates the Gravity, Rotation, and Deformation (GRD) effects resulting from

https://doi.org/10.5194/egusphere-2026-4642
Preprint. Discussion started: 7 August 2026

Present-Day Ice Melting (PDIM). These corrections ensure that altimetric observations are physically consistent with gravimetric manometric estimates and in-situ steric measurements within the sea level budget framework.

The input data consist of the following components:

Input data	Acronym	Sources
Geocentric sea level component (also called absolute)	ΔSL_{abs}	The absolute sea level change at regional scales are derived from the sea-level product operationally generated by the Copernicus Climate Change Service (Legeais et al., 2021). The multi satellite sea-level maps have a spatial resolution of 1/4° × 1/4° on a Mercator grid with a 1-day interval.
Manometric sea level component corrected for GIA	ΔSL_{man}	Manometric sea level change estimates are derived from gravimetric measurements (GRACE(-FO)) from the AVISO+ ensemble (Blazquez et al., 2018). The manometric sea level is corrected for GIA using the correction from Spada & Melini, 2019.
Vertical Land Motion component	ΔVLM	Glacial isostatic adjustment (GIA) and recent ice melting corrections from Spada & Melini, 2019.
Steric sea level component from in-situ data	ΔSL_{steric}	Steric Sea Level derived from gridded interpolated temperature and salinity profiles from the Argo network (Kolodziejczyk et al., 2023) is computed using the Thermodynamic Equation of Seawater 2010 (TOES10 Gibbs Seawater toolbox).

Table F1: Input data used in the current SLB product over the period 2002-2022 equations

Computations of SLB residuals

The SLB residuals (r) represent the discrepancy between the total observed sea level and the sum of its physical components. This is assessed at both regional and global scales.

At the grid level, the residuals are calculated as the difference between absolute sea level and the sum of the manometric, steric, and GIA-related vertical land motion components:

$$r = \Delta SL_{abs} - \Delta SL_{man} - \Delta SL_{steric} - \Delta VLM \quad \text{(F1)}$$

https://doi.org/10.5194/egusphere-2026-4642
Preprint. Discussion started: 7 August 2026

Where ΔSL_{abs} is the absolute sea level change, ΔSL_{man} is the manometric sea level (excluding GIA effects), SL_{steric} is the total steric component (thermosteric + halosteric), and ΔVLM represents the correction for glacial isostatic adjustment and associated seafloor deformation.

Computation of the comparison metrics

The realization of the error in the SLB residuals at regional scales, due to errors in manometric sea level change arising from ocean mass change, is estimated for each scenario using the following method:

- Calculate the difference between the manometric sea level change from the simulation and the manometric sea level change from the ocean model (assumed to be the true value):

$$e\Delta SL_{man} = SL_{man}^{sim} - SL_{man}^{ESM} \quad \text{(F2)}$$

With eΔSL_{man} the error realisation for a specific configuration, SL_{man}^{sim} the manometric sea level change simulated for a specific satellite configuration and SL_{man}^{ESM} the manometric sea level changes from the reference (here, ESA ESM2.0 HIS).

- Retrieving to the absolute sea level the sum of the contribution of each component involved in the current sea level budget. This calculation is performed regionally on a 1°x 1° grid over the entire 12-year simulation period. The sea level budget residuals are computed from the sea level budget components as follows:

$$SL_{res} = (\Delta SL_{abs})_{alti} - \left(\Delta SL_{man_{GIA}}\right)_{gravi} - (\Delta SL_{thermo} + \Delta SL_{halo})_{insitu} - \Delta VLM_{current} - N_{GIA} \quad \text{(F3)}$$

With SL_{res} the sea level budget residuals obtained using the current system observations, $(\Delta SL_{abs})_{alti}$, the absolute sea level estimated by altimetry, $\left(\Delta SL_{man_{GIA}}\right)_{gravi}$, the L3 manometric sea level estimated by GRACE and GRACE-FO corrected for GIA, $(\Delta SL_{thermo} + \Delta SL_{halo})_{insitu}$, the thermosteric and halosteric sea level estimated by in situ observations and N_{GIA} and $\Delta VLM_{current}$ the corrections related to GIA and present day ice melting for absolute sea level, respectively.

- Comparing the error realisation on the manometric sea level simulated with the SLB residual estimates generated by the current statutory system observation. The key metrics used for this evaluation are the error ratios (R_{sim} and R_{curr}), which help quantify the magnitude of errors in the manometric sea level change with respect to the SLB residuals:

$$R_{sim} = \left|\frac{e\Delta SL_{man}^{sim}}{SLres}\right| \quad \text{(F4)}$$

And,

$$R_{curr} = \left|\frac{e\Delta SL_{man}^{curr}}{SLres}\right|$$

(F5)

With R_{sim} the ratio estimated using the simulations and R_{curr} the ratio estimated using the current system observations $e\Delta SL_{man}^{curr}$, the current uncertainty on GRACE and GRACE-FO data).

https://doi.org/10.5194/egusphere-2026-4642
Preprint. Discussion started: 7 August 2026

Key metrics

These comparisons are conducted for each scenario over different time periods. The simulated data covers the period 1995–2006, so we propose to compare it with observational data from a completely different 12-year period (2011–2022) to assess robustness. Additionally, we evaluated the impact of the comparison period by including a shorter 4-year period (2003–2006), which corresponds to a key damage phase. The key metrics computed in this context are as follows:

- Annual amplitude of the error ratios at regional and global scale: the annual amplitude of the error ratios will help to quantify the contribution of the errors from satellite gravity missions to the non-closure of the sea level budget at annual timescales
- Linear trend of the error ratios at regional and global scale: the linear trend of the error ratios calculated over the 12 years of the observation period will help to quantify the contribution of the errors from satellite gravity missions to the non-closure of the sea level budget at decadal timescales
- Standard deviation of detrended and deseasoned error ratios at regional and global scale: The standard deviation of the error ratios over the 12 years will help quantify the contribution of the errors from satellite gravity missions to the non-closure of the sea level budget at high frequencies and interannual timescales

By comparing the error ratios (R_{sim} and R_{curr}), obtained from each scenario (GRACE-C, NGGM, MAGIC) with real data, we can evaluate the relative effectiveness of each mission in reducing uncertainties and improving the accuracy of SLB residual estimates.

Appendix G: Glaciology

Extended description of the methods used to assess the improved capabilities of the NGGM and MAGIC missions for the cryosphere.

Noise estimate from closed-loop simulations

All analyses use a seven-basin partition of Greenland and a 25-basin partition of Antarctica defined by major ice divides (Sasgen et al., 2012, 2013), consistent with the IMBIE drainage systems (The IMBIE Team, 2020). Gravity-mission data are based on the closed-loop simulations for the MAGIC dual-pair constellation and its near-polar GRACE-C-like and 70°-inclined NGGM pairs ESM2.0 truth fields (Dobslaw et al., 2015). Five-day retrievals (1995–2016) to degree and order 70 are used for the sub-monthly surface-mass-balance (SMB) assessment. Residuals between recovered and truth coefficients, $\Delta\sigma_{jm}(t)$. As NGGM does not sample poleward of 70°; a polar-cap regularisation is applied, and basins with <2% NGGM coverage are excluded from NGGM-only analyses.

Detectability of sub-monthly SMB variability

Daily SMB is taken from MAR v3.12 for Greenland (20 km, ERA5-forced, 1950–2020; Fettweis et al., 2017) and MAR v3.6 for Antarctica (35 km, ERA-Interim-forced, 1979–2018; Agosta et al., 2019); ice-dynamic discharge is neglected at these time scales (King et al., 2018). The retrieval period n (days) is a free parameter. Basin-integrated daily SMB $s_b(i)$ is summed over non-overlapping n-day windows,

$$S_b^{(n)}(k) = \sum_{l=0}^{n-1} \quad s_b(k+l), \tag{G1}$$

anomalies are formed relative to the long-term climatological mean, and their standard deviation defines the signal amplitude $V_b(n)$. We quantify the temporal omission errors as $E_b(n) = V_b(n)/V_b(1)$. For the noise, residuals $\Delta\sigma_{jm}(t)$ are low-pass filtered (moving average over eight 5-day solutions), narrowband peaks at 5, 10 and 15 days are attenuated, and basin-integrated noise is computed by spectral basin averaging (Wahr et al., 1998),

$$M_b(t) = K \sum_{j=0}^{j_{max}} \quad \sum_{m=-j}^{j} \quad \Delta\sigma_{jm}(t)\, W_{jm}^{(b)}, \tag{G2}$$

whose standard deviation gives $N_b(n_0)$ at native sampling (n_0 = 5 days for simulations). Assuming uncorrelated errors, $N_b(n) = N_b(n_0)\sqrt{n_0/n}$, with a factor $\sqrt{2}$ for flux differencing. The detection limit is the shortest n at which signal variance exceeds noise variance; spatially, the criterion $S_g(n) > N_g(n)$ is applied to gridded fields truncated at degree 70.

Appendix H: Climate sciences

To assess the influence of the GRACE-C, NGGM, and MAGIC missions on OHC and EEI error budgets, we evaluate the error realizations associated with OHC and EEI estimates under the three mission configurations. In this study, we use L3b (VADER-filtered) monthly simulations from the SING dataset. This approach quantifies the contribution of mission-specific error realizations to the discrepancies observed in OHC and EEI estimates. The resulting relative impact is then compared with OHC and EEI estimates derived from real data across a range of temporal scales, from 1 to 10 years.

The realization of the error in regional OHC change, arising from errors in manometric sea level change associated with ocean mass variations, is computed as described in Eq. (1). First, the difference between the simulated manometric sea level change and the reference signal (here, ESM2.0-HIS) is calculated. Second, this difference is divided by the IEEH coefficient estimated from ECCO-V4r4 to obtain the OHC change error realization (ΔOHC_{error}). This calculation is performed regionally on a 1° × 1° grid over the full 12-year simulation period, after applying a low-pass filter to remove variability at periods shorter than 2 years.

$$\Delta OHC_{error} = \frac{SL_{man\,(from\,simulation)} - \Delta SL_{man\,(from\,ocean\,model)}}{IEEH} \tag{H1}$$

The realization of the error in ocean heat uptake (OHU_{error}) is calculated by calculating the time derivative of the realization of the error in the OHC change.

https://doi.org/10.5194/egusphere-2026-4642
Preprint. Discussion started: 7 August 2026

a) At regional scale, the equation is:

$$OHU_{error} = \frac{d}{dt}\,(\Delta OHC_{error}) \quad \text{(H2)}$$

b) At the global scale, the regional error in OHC change must be summed up before calculating the error in the global ocean heat uptake ($GOHU_{error}$):

$$GOHU_{error} = \frac{d}{dt}\left(\left(\sum_{lat,lon} \Delta OHC_{error}\right)\right) \quad \text{(H3)}$$

The error in EEI estimates are computed by dividing the error in the error in the global ocean heat uptake by coefficient representing the ocean's capacity to absorb excess energy from the Earth in the form of heat (α) .

$$EEI_{error} = \frac{GOHU_{error}}{\alpha} \quad \text{(H4)}$$

In summary, we analyze differences in OHC and EEI changes estimated from manometric sea level variations by comparing results from GRACE-C, NGGM, and MAGIC mission simulations with those derived from ocean model estimates. These differences are then evaluated against OHC and EEI estimates provided by the MOHeaCAN space geodetic product (https://doi.org/10.24400/527896/a01-2020.003).

Appendix I: Solid Earth Sciences

Recent analyses of GRACE and GRACE-FO observations demonstrated the detectability of co-seismic gravity signals for large earthquakes ($Mw \geqslant 8.5$). In this work, we assess the capability of the NGGM and MAGIC mission concepts to detect and characterize earthquake-related gravity variations connected to this type of event with magnitude (Mw 8.5), and compare their performance with GRACE-C simulations. Synthetic co-seismic and post-seismic gravity signals are generated using a point source. The simulations include thrust and strike-slip mechanisms in continental tectonic environments. Finite-fault models are constructed using empirical scaling relationships between seismic moment and rupture dimensions (Wells & Coppersmith, 1994). For representative subduction-zone scenarios, we simulate Mw 8.0 – 8.5 thrust earthquakes with variable fault geometry, slip distribution, and rheological structure. Post-seismic relaxation is computed assuming a layered viscoelastic Earth model including an elastic lithosphere, a Burgers-type asthenosphere, and Maxwell rheology in the deeper mantle Table I1.

Table I1: Rheological properties of Earth layers

Layer No.	Depth (km)	Vp (km s^{-1})	Vs (km s^{-1})	ρ (g cm^{-3})	η_1 (Pa·s)	η_2 (Pa·s)	α (–)	Remark

https://doi.org/10.5194/egusphere-2026-4642
Preprint. Discussion started: 7 August 2026

1	0.0	5.8	3.36	2.72	0.00E+00	0.00E+00	1.0	Hooke
2	20.0	5.8	3.36	2.72	0.00E+00	0.00E+00	1.0	
3	20.0	6.5	3.75	2.92	0.00E+00	0.00E+00	1.0	
4	35.0	6.5	3.75	2.92	0.00E+00	0.00E+00	1.0	
5	35.0	8.04	4.47	3.32	0.00E+00	0.00E+00	1.0	
6	40.0	8.041	4.472	3.323	0.00E+00	0.00E+00	1.0	Hooke
7	40.0	8.041	4.472	3.323	1.00E+18	1.00E+19	0.5	Burgers
8	120.0	8.05	4.5	3.371	1.00E+18	1.00E+19	0.5	
9	210.0	8.3	4.518	3.426	1.00E+18	1.00E+19	0.5	Burgers
10	210.0	8.3	4.522	3.426	0.00E+00	1.00E+20	1.0	Maxwell A
11	410.0	9.03	4.87	3.547	0.00E+00	1.00E+20	1.0	
12	410.0	9.36	5.07	3.756	0.00E+00	1.00E+20	1.0	
13	660.0	10.2	5.6	4.065	0.00E+00	1.00E+20	1.0	Maxwell A
14	660.0	10.79	5.95	4.371	0.00E+00	1.00E+21	1.0	Maxwell B
15	760.0	11.056	6.209	4.431	0.00E+00	1.00E+21	1.0	

https://doi.org/10.5194/egusphere-2026-4642
Preprint. Discussion started: 7 August 2026

16	1000.0	11.464	6.384	4.5698	0.00E+00	1.00E+21	1.0	
17	1200.0	11.771	6.512	4.6839	0.00E+00	1.00E+21	1.0	
18	1400.0	12.052	6.627	4.7951	0.00E+00	1.00E+21	1.0	Maxwell B

Detectability is evaluated by comparing localized spherical harmonic spectra of earthquake gravity signals with simulated retrieval-error spectra from GRACE-C, NGGM, and MAGIC mission simulations (TUM). Localization following Wieczorek & Simons (2005) is applied to account for the spatially localized nature of earthquake gravity signals. The analysis is performed for both unfiltered and VADER-filtered solutions at 5-day and monthly temporal sampling.

Appendix J: Evaluation of Mission Contributions to IHRF Realization

The International Association of Geodesy (IAG) established in 2015 the International Height Reference System (IHRS), a global and unified standard for the precise determination of physical heights. The realization of this system is achieved through the International Height Reference Frame (IHRF), which requires a precise (at the 1 cm2/s2 and 0.1 cm2/s2/a) determination of gravity potential values, along with their temporal evolution, directly at physical reference stations distributed globally on the Earth's surface. Consequently, its sustainability, maintenance, and accuracy inherently rely on high-resolution global gravity field models provided by future satellite gravity missions, such as NGGM/MAGIC.

To quantitatively evaluate the expected contribution of the simulated mission scenarios (GRACE-C, NGGM, and MAGIC) to the IHRF, the methodology relies on the computation of Level-4 data products at IHRF stations referring to variations and trends of gravity potential, geoid height, physical height, and ellipsoidal height. The former are evaluated over 12 core IHRF reference stations (namely, ADIS, AUT1, CUIB, EUR2, MKEA, NRIL, OHI3, SCH2, SG27_ngs, SHAO, STR2, and SYOG), as presented in Figure J1. The foundational input for this process consists of Vader-filtered Level-2b simulated Spherical Harmonic Coefficients (SHCs) of the Earth's gravity field, provided up to degree and order 120 and spanning a 12-year simulation period (1995–2006).

To assess the influence of the GRACE-C, NGGM, and MAGIC missions on the IHRF, an evaluation of the missions' geodetic performance is conducted by extracting the time-series residuals between these Level-4 data and the respective values derived directly from the Earth System Model 2.0 (specifically the ESM2.0), which serves as the absolute ground truth for the various evaluations. This direct validation allows for a precise quantification of the added value that the NGGM and MAGIC constellations bring to the accuracy of the global height reference frame.

https://doi.org/10.5194/egusphere-2026-4642
Preprint. Discussion started: 7 August 2026

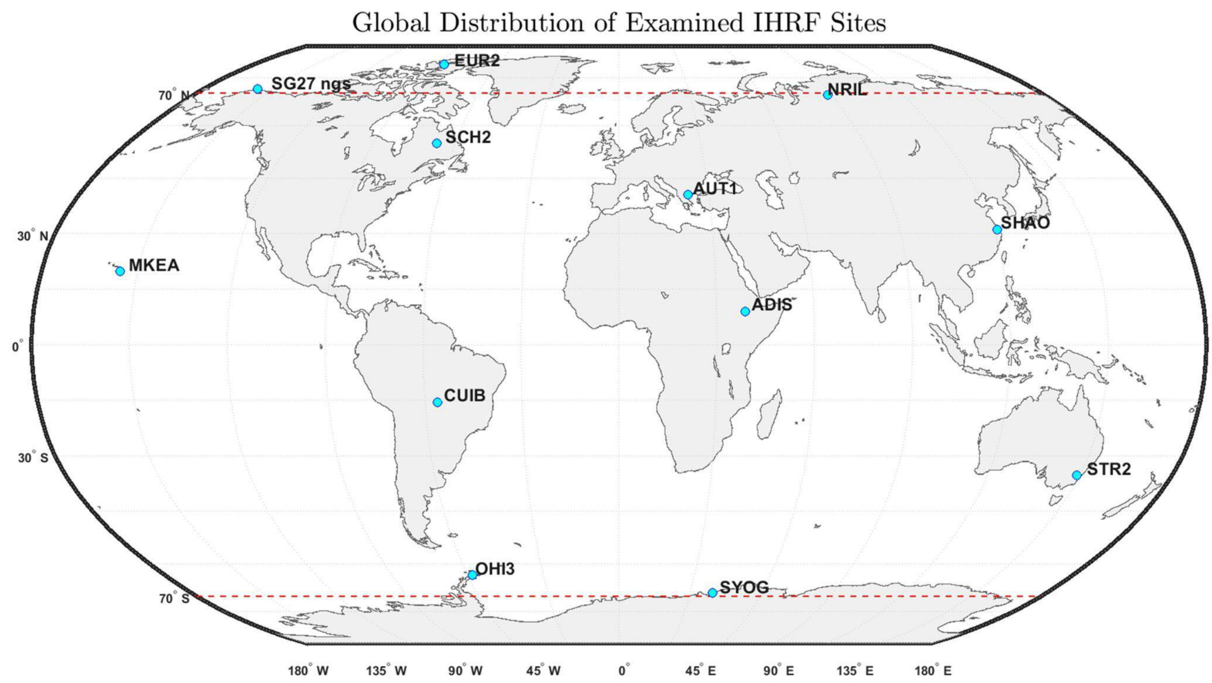

Figure J1: Global distribution of the 12 examined IHRF reference stations.

Code and data availability

The ESA Earth System Model version 2.0 (ESA ESM2.0), described by Dobslaw et al. (2015) and used as the reference dataset in this study, is publicly available through the ISDC data portal at https://isdc-data.gfz.de/future_missions/esaesm/ESAESM2/. The Level-2 and Level-3 ESA SING datasets (Schlaak et al., 2026), including simulations for the GRACE-C, NGGM, and MAGIC gravity mission scenarios, are publicly available through the ISDC data portal at https://isdc-data.gfz.de/future_missions/. The corresponding dataset is archived by GFZ Data Services and is available at https://doi.org/10.5880/fidgeo.2026.049. The Level-4 (L4) products generated in this study will be deposited in a FAIR-compliant public data repository and assigned a persistent identifier (DOI) upon acceptance of the manuscript. The DOI and repository information will be added to this section before final publication. During the peer-review process, the L4 products are available to reviewers upon request from the corresponding author.

Author contributions

JP coordinated the project and led the preparation of the manuscript. BM was the scientific lead of the project. RP coordinated the data simulation activities. ID supervised the project on behalf of ESA. MB, RF, RB, JK, EF, LB, MJT, IS, BW, IP, CB,

https://doi.org/10.5194/egusphere-2026-4642
Preprint. Discussion started: 7 August 2026

and GV led the scientific investigations in their respective research areas. HG, FY, MSchu MUL, FL, AS, NS, PS, AK, MTJ, GM, DT, TP, EM, AB, MSchl, HD, LS, VK, and LJ contributed to the investigation, methodology, formal analysis, software development, data curation, validation, and visualization, as appropriate. GL supported the project administration and coordination. All authors contributed to writing, reviewing, and editing the manuscript, discussed the results, and approved the final version.

Competing interests

Luca Brocca is an editor of Earth Observation (EO). To avoid any conflict of interest, he will not be involved in the editorial process for this manuscript. The remaining authors declare that they have no competing interests.

Disclaimer

Copernicus Publications remains neutral with regard to jurisdictional claims made in the text, published maps, institutional affiliations, or any other geographical representation in this paper. While Copernicus Publications makes every effort to include appropriate place names, the final responsibility lies with the authors. Views expressed in the text are those of the authors and do not necessarily reflect the views of the publisher.

Acknowledgements

The authors used an artificial intelligence–based writing assistant exclusively for language editing, including grammar, spelling, and readability improvements. The conception of the study, scientific analyses, results, interpretations, and conclusions are the authors' own. All AI-generated suggestions were carefully reviewed, revised where appropriate, and approved by the authors, who assume full responsibility for the final manuscript.

Financial support

This work was carried out within the SING project (https://www.esa-sing.org/), funded by the European Space Agency under the ‘NGGM and MAGIC Science and Applications Impact Study’ ESA Contract No. 4000145265/24/NL/SC. Anne Springer and Jürgen Kusche acknowledge partial support by the German Research Foundation (DFG), SFB 1502/1-2022, project number 450058266.

https://doi.org/10.5194/egusphere-2026-4642
Preprint. Discussion started: 7 August 2026

References

Agosta, C., Amory, C., Kittel, C., Orsi, A., Favier, V., Gallée, H., van den Broeke, M. R., Lenaerts, J. T. M., van Wessem, J. M., van de Berg, W. J., and Fettweis, X.: Estimation of the Antarctic surface mass balance using the regional climate model MAR (1979–2015) and identification of dominant processes, The Cryosphere, 13, 281–296, https://doi.org/10.5194/tc-13-281-2019, 2019.

Aschwanden, A., Bartholomaus, T. C., Brinkerhoff, D. J., and Truffer, M.: Brief communication: A roadmap towards credible projections of ice sheet contribution to sea level, The Cryosphere, 15, 5705–5715, https://doi.org/10.5194/tc-15-5705-2021, 2021.

Bouih, M., Barnoud, A., Yang, C., Storto, A., Blazquez, A., Llovel, W., Fraudeau, R., and Cazenave, A.: Regional sea level trend budget over 2004–2022, Ocean Sci., 21, 1425–1440, https://doi.org/10.5194/os-21-1425-2025, 2025.

Blazquez, A., Meyssignac, B., Lemoine, J.-M., Ribes, A., Berthier, E., and Cazenave, A.: Exploring the uncertainty in GRACE estimates of the mass redistributions at the Earth surface: Implications for the global water and sea level budgets, Geophys. J. Int., 215, 415–430, https://doi.org/10.1093/gji/ggy293, 2018.

Brocca, L., Massari, C., Ciabatta, L., Moramarco, T., Penna, D., Zuecco, G., Pianezzola, L., Borga, M., Matgen, P., and Martínez-Fernández, J.: Rainfall estimation from in situ soil moisture observations at several sites in Europe: An evaluation of the SM2RAIN algorithm, J. Hydrol. Hydromech., 63, 201–209, https://doi.org/10.1515/johh-2015-0016, 2015.

Brodeau, L., Barnier, B., Treguier, A.-M., Penduff, T., and Gulev, S.: An ERA40-based atmospheric forcing for global ocean circulation models, Ocean Model., 31, 88–104, https://doi.org/10.1016/j.ocemod.2009.10.005, 2010.

Chao, B. F. and Liau, J. R.: Gravity changes due to large earthquakes detected in GRACE satellite data via empirical orthogonal function analysis, J. Geophys. Res.: Solid Earth, 124, 3024–3035,https://doi.org/10.1029/2018JB016862, 2019.

Chen, J., Cazenave, A., Dahle, C., Llovel, W., Panet, I., Pfeffer, J., and Moreira, L.: Applications and Challenges of GRACE and GRACE Follow-On Satellite Gravimetry, Surv. Geophys., 43, 305–345, https://doi.org/10.1007/s10712-021-09685-x, 2022.

Daras, I. (Ed.): Next Generation Gravity Mission (NGGM) Mission Requirements Document, European Space Agency, Earth and Mission Science Division, Issue 2.0 Draft version dated 3.3.2026, 2026.

Daras, I., March, G., Pail, R., Hughes, C. W., Braitenberg, C., Güntner, A., Eicker, A., Wouters, B., Heller-Kaikov, B., Pivetta, T., and Pastorutti, A.: Mass-change And Geosciences International Constellation (MAGIC) expected impact on science and applications, Geophys. J. Int., 236, 1288–1308, https://doi.org/10.1093/gji/ggad472, 2024.

Dee, D. P., Uppala, S. M., Simmons, A. J., Berrisford, P., Poli, P., Kobayashi, S., … and Vitart, F.: The ERA-Interim reanalysis: configuration and performance of the data assimilation system, Q. J. R. Meteorol. Soc., 137, 553–597, https://doi.org/10.10 02/qj.828, 2011.

https://doi.org/10.5194/egusphere-2026-4642
Preprint. Discussion started: 7 August 2026

Dobslaw, H., Bergmann-Wolf, I., Dill, R., Forootan, E., Klemann, V., Kusche, J., and Sasgen, I.: The updated ESA Earth System Model for future gravity mission simulation studies, J. Geod., 89, 505–513, https://doi.org/10.1007/s00190-014-0787-8, 2015.

Dobslaw, H., Bergmann-Wolf, I., Forootan, E., Dahle, C., Mayer-Gürr, T., Kusche, J., and Flechtner, F.: Modeling of present-day atmosphere and ocean non-tidal de-aliasing errors for future gravity mission simulations, J. Geod., 90, 423–436, https://doi.org/10.1007/s00190-015-0884-3, 2016.

Dussin, R., Barnier, B., Brodeau, L., and Molines, J.-M.: The making of the DRAKKAR Forcing Set DFS5, Zenodo [report], https://doi.org/10.5281/zenodo.1209243, 2018

European Commission Joint Research Centre: European Drought Observatory map, Copernicus Emergency Management Service, https://drought.emergency.copernicus.eu/tumbo/edo/map/ (last access: 11 December 2025).

European Commission Joint Research Centre: Global Drought Observatory map, Copernicus Emergency Management Service, https://drought.emergency.copernicus.eu/tumbo/gdo/map/ (last access: 11 December 2025).

European Space Agency, Haagmans, R., Tsaoussi, L., NASA, Massotti, L., European Space Agency, March, G., European Space Agency, Daras, I., and European Space Agency: Next Generation Gravity Mission as a Mass-change And Geosciences International Constellation (MAGIC) Mission Requirements Document (1.0), European Space Agency, https://doi.org/10.5270/esa.nasa.magic-mrd.2020, 2020.

Fettweis, X., Box, J. E., Agosta, C., Amory, C., Kittel, C., Lang, C., Van As, D., Machguth, H., and Gallée, H.: Reconstructions of the 1900–2015 Greenland ice sheet surface mass balance using the regional climate MAR model, The Cryosphere, 11, 1015–1033, https://doi.org/10.5194/tc-11-1015-2017, 2017.

Fettweis, X., Hofer, S., Krebs-Kanzow, U., Amory, C., Aoki, T., Berends, C. J., Born, A., Box, J. E., Delhasse, A., Fujita, K., Gierz, P., Goelzer, H., Hanna, E., Hashimoto, A., Huybrechts, P., Kapsch, M.-L., King, M. D., Kittel, C., Lang, C., and Zolles, T.: GrSMBMIP: Intercomparison of the modelled 1980–2012 surface mass balance over the Greenland Ice Sheet, The Cryosphere, 14, 3935–3958, https://doi.org/10.5194/tc-14-3935-2020, 2020.

Fettweis, X. and Mattingly, K.: Modèle Atmosphérique Régional (MAR) v3.12.0 15 km output for Greenland (JJA 1980–2020, 1-hourly), Zenodo [data set], https://doi.org/10.5281/ZENODO.7591112, 2023.

Forootan, E., Mehrnegar, N., Schumacher, M., Schiettekatte, L. A. R., Jagdhuber, T., Farzaneh, S., Van Dijk, A. I. J. M., Shamsudduha, M., and Shum, C. K.: Global groundwater droughts are more severe than they appear in hydrological models: An investigation through a Bayesian merging of GRACE and GRACE-FO data with a water balance model, Sci. Total Environ., 912, 169476, https://doi.org/10.1016/j.scitotenv.2023.169476, 2024.

Fox-Kemper, B., Hewitt, H. T., Xiao, C., Adalgeirsdottir, G., Drijfhout, S. S., Edwards, T. L., Golledge, N. R., Hemer, M., Kopp, R. E., Krinner, G., Mix, A., Notz, D., Nowicki, S., Nurhati, I. S., Ruiz, L., Sallée, J.-B., Slangen, A. B. A., and Yu, Y.: Ocean, Cryosphere and Sea Level Change, in: Climate Change 2021: The Physical Science Basis. Contribution of Working Group I to the Sixth Assessment Report of the Intergovernmental Panel on Climate Change, edited by: Masson-Delmotte, V., Zhai, P., Pirani, A., Connors, S. L., Péan, C., Berger, S., Caud, N., Chen, Y., Goldfarb, L., Gomis, M. I., Huang, M., Leitzell,

https://doi.org/10.5194/egusphere-2026-4642
Preprint. Discussion started: 7 August 2026

K., Lonnoy, E., Matthews, J. B. R., Maycock, T. K., Waterfield, T., Yelekci, O., Yu, R., and Zhou, B., Cambridge University Press, 1211–1362, https://doi.org/10.1017/9781009157896.011, 2021.

Fricker, H. A., Galton-Fenzi, B. K., Walker, C. C., Freer, B. I. D., Padman, L., and DeConto, R.: Antarctica in 2025: Drivers of deep uncertainty in projected ice loss, Science, 387, 601–609, https://doi.org/10.1126/science.adt9619, 2025.

Gerdener, H.: A global drought monitoring framework using GRACE/-FO data assimilation, Ph.D. thesis, Rheinische Friedrich-Wilhelms-Universität Bonn, https://doi.org/10.48565/BONNDOC-438, 2024.

Gerdener, H., Kusche, J., Schulze, K., Döll, P., and Klos, A.: The global land water storage data set release 2 (GLWS2.0) derived via assimilating GRACE and GRACE-FO data into a global hydrological model, J. Geod., 97, 73, https://doi.org/10.1007/s00190-023-01763-9, 2023.

Heller-Kaikov, B., Pail, R., and Daras, I.: Mission design aspects for the mass change and geoscience international constellation (MAGIC), Geophys. J. Int., 235, 718–735, https://doi.org/10.1093/gji/ggad266, 2023.

Horvath, A., Murböck, M., Pail, R., and Horwath, M.: Decorrelation of GRACE Time Variable Gravity Field Solutions Using Full Covariance Information, Geosciences, 8, Article 9, https://doi.org/10.3390/geosciences8090323, 2018.

Huai, B., Ding, M., van den Broeke, M. R., Reijmer, C. H., Noël, B., Sun, W., and Wang, Y.: Future large-scale atmospheric circulation changes and Greenland precipitation, npj Clim. Atmos. Sci., 8, 10, https://doi.org/10.1038/s41612-025-00899-z, 2025.

King, M. D., Howat, I. M., Jeong, S., Noh, M. J., Wouters, B., Noël, B., and van den Broeke, M. R.: Seasonal to decadal variability in ice discharge from the Greenland Ice Sheet, The Cryosphere, 12, 3813–3825, https://doi.org/10.5194/tc-12-3813-2018, 2018.

Kolodziejczyk, N., Prigent-Mazella, A., and Gaillard, F.: ISAS temperature, salinity, dissolved oxygen gridded fields, SEANOE [data set], https://doi.org/10.17882/52367, 2023.

Kopp, R. E., Oppenheimer, M., O'Reilly, J. L., Drijfhout, S. S., Edwards, T. L., Fox-Kemper, B., Garner, G. G., Golledge, N. R., Hermans, T. H. J., Hewitt, H. T., Horton, B. P., Krinner, G., Notz, D., Nowicki, S., Palmer, M. D., Slangen, A. B. A., and Xiao, C.: Communicating future sea-level rise uncertainty and ambiguity to assessment users, Nat. Clim. Change, 13, 648–660, https://doi.org/10.1038/s41558-023-01691-8, 2023.

Kusche, J., Eicker, A., Forootan, E., Springer, A., and Longuevergne, L.: Mapping probabilities of extreme continental water storage changes from space gravimetry, Geophys. Res. Lett., 43, 8026–8034, https://doi.org/10.1002/2016GL069538, 2016.

Landerer, F. W., Flechtner, F. M., Save, H., Webb, F. H., Bandikova, T., Bertiger, W. I., Bettadpur, S. V., Byun, S. H., Dahle, C., Dobslaw, H., Fahnestock, E., Harvey, N., Kang, Z., Kruizinga, G. L. H., Loomis, B. D., McCullough, C., Murböck, M., Nagel, P., Paik, M., and Yuan, D.-N.: Extending the Global Mass Change Data Record: GRACE Follow-On Instrument and Science Data Performance, Geophys. Res. Lett., 47, e2020GL088306, https://doi.org/10.1029/2020GL088306, 2020.

Legeais, J.-F., Meyssignac, B., Faugère, Y., Guerou, A., Ablain, M., Pujol, M.-I., Dufau, C., and Dibarboure, G.: Copernicus sea level space observations: A basis for assessing mitigation and developing adaptation strategies to sea level rise, Front. Mar. Sci., 8, 704721, doi: 10.3389/fmars.2021.704721, 2021.

https://doi.org/10.5194/egusphere-2026-4642
Preprint. Discussion started: 7 August 2026

Maclennan, M. L., Winters, A. C., Shields, C. A., Thaker, R., Barthelemy, L., Codron, F., and Wille, J. D.: Rising atmospheric moisture escalates the future impact of atmospheric rivers in the Antarctic climate system, Commun. Earth Environ., 6, 369, https://doi.org/10.1038/s43247-025-02333-x, 2025.

Marti, F., Blazquez, A., Meyssignac, B., Ablain, M., Barnoud, A., Fraudeau, R., Jugier, R., Chenal, J., Larnicol, G., Pfeffer, J., Restano, M., and Benveniste, J.: Monitoring the ocean heat content change and the Earth energy imbalance from space altimetry and space gravimetry, Earth Syst. Sci. Data, 14, 229–249, https://doi.org/10.5194/essd-14-229-2022, 2022.

Marzocchi, A., Hirschi, J. J.-M., Holliday, N. P., Cunningham, S. A., Blaker, A. T., and Coward, A. C.: The North Atlantic subpolar circulation in an eddy-resolving global ocean model, J. Mar. Syst., 142, 126–143, https://doi.org/10.1016/j.jmarsys.2014.10.007, 2015.

Meyssignac, B., Boyer, T., Zhao, Z., Hakuba, M. Z., Landerer, F. W., Stammer, D., Köhl, A., Kato, S., L'Ecuyer, T., Ablain, M., Abraham, J. P., Blazquez, A., Cazenave, A., Church, J. A., Cowley, R., Cheng, L., Domingues, C. M., Giglio, D., Gouretski, V., and Zilberman, N.: Measuring Global Ocean Heat Content to Estimate the Earth Energy Imbalance, Front. Mar. Sci., 6, 432, https://doi.org/10.3389/fmars.2019.00432, 2019.

Murböck, M.: Virtual Constellations of Next Generation Gravity Missions, Ph.D. thesis, Technische Universität München, https://mediatum.ub.tum.de/1241150, 2015.

Oppenheimer, M., Glavovic, J., Hinkel, J., van de Wal, R. S. W., Magnan, A., Abd-Elgawad, A., Cai, R., Cifuentes-Jara, R. M., DeConto, R., Ghosh, J., Hay, J., Isla, F., Marzeion, B., Meyssignac, B., and Sebesvari, Z.: Sea Level Rise and Implications for Low-Lying Islands, Coasts and Communities, in: IPCC Special Report on the Ocean and Cryosphere in a Changing Climate (SROCC), edited by: Pörtner, H.-O., Roberts, D. C., Masson-Delmotte, V., Zhai, P., Tignor, M., Poloczanska, E., Mintenbeck, K., Alegría, A., Nicolai, M., Okem, A., Petzold, J., Rama, B., and Weyer, N. M., Cambridge University Press, 321–345, https://doi.org/10.1017/9781009157964.006, 2023.

World Meteorological Organization (WMO), United Nations Environment Programme (UNEP), International Science Council (ISC), and Intergovernmental Oceanographic Commission of UNESCO (IOC): The 2022 GCOS Implementation Plan (GCOS-244), https://library.wmo.int/records/item/58104-the-2022-gcos-implementation-plan-gcos-244 (last access: 3 December 2025).

Pail, R. (Ed.), Gruber, T., Abrykosov, P., Zingerle, P., Visser, P., Teixeira da Encarnação, J., Siemes, C., Flechtner, F., Dahle, C., Hauk, M., Wilms, J., Bruinsma, S., Marty, J.-C., Müller, V., and Müller, L.: NGGM/MAGIC – Science Support Study during Phase A, Final Report, ESA/ESTEC Contract No. 4000134613/21/NL/FF/ab, https://www.asg.ed.tum.de/iapg/magic/documents/, 2022.

Pail, R., Gruber, T., Abrykosov, P., Zingerle, P., Visser, P., Teixeira da Encarnação, J., Siemes, C., Flechtner, F., Dahle, C., Hauk, M., Wilms, J., Bruinsma, S., Marty, J.-C., Müller, V., and Müller, L.: ATBD of NGGM/MAGIC L2 and L3 Products, Issue 2.0, Technical Report MAGIC_TR_D1-CCN1, ESA/ESTEC Contract No. 4000134613/21/NL/FF/ab, Technische Universität München, 2023

https://doi.org/10.5194/egusphere-2026-4642
Preprint. Discussion started: 7 August 2026

Pail, R., Bingham, R., Braitenberg, C., Dobslaw, H., Eicker, A., Güntner, A., Horwath, M., Ivins, E., Longuevergne, L., Panet, I., Wouters, B., and IUGG Expert Panel: Science and User Needs for Observing Global Mass Transport to Understand Global Change and to Benefit Society, Surv. Geophys., 36, 743–772, https://doi.org/10.1007/s10712-015-9348-9, 2015.

Panet, I., Bonvalot, S., Narteau, C., Rémy, D., and Lemoine, J.-M.: Migrating pattern of deformation prior to the Tohoku-Oki earthquake revealed by GRACE data, Nat. Geosci., 11, 367–373, https://doi.org/10.1038/s41561-018-0099-3, 2018.

Panet, I., Mikhailov, V., Diament, M., Pollitz, F., King, G., de Viron, O., Holschneider, M., Biancale, R., and Lemoine, J.-M.: Coseismic and post-seismic signatures of the Sumatra 2004 December and 2005 March earthquakes in GRACE satellite gravity, Geophys. J. Int., 171, 177–190, https://doi.org/10.1111/j.1365-246X.2007.03525.x, 2007.

Ray, R. D.: A Global Ocean Tide Model from TOPEX/Poseidon Altimetry: GOT99.2, NASA Technical Memorandum 209478, Goddard Space Flight Center, Greenbelt, MD, USA, 1999 (Model version GOT4.7 used).

Sánchez, L., Barzaghi, R., and Vergos, G.: Operational Infrastructure to Ensure the Long-Term Sustainability of the International Height Reference System and Frame (IHRS/IHRF), in: Together Again for Geodesy, Vol. 157, edited by: Freymueller, J. T. and Sánchez, L., Springer Nature Switzerland, 263–272, https://doi.org/10.1007/1345_2024_250, 2024.

Sasgen, I., van den Broeke, M. R., Bamber, J. L., Rignot, E., Sørensen, L. S., Wouters, B., Martinec, Z., Velicogna, I., and Simonsen, S. B.: Timing and origin of recent regional ice-mass loss in Greenland, Earth Planet. Sci. Lett., 333–334, 293–303, https://doi.org/10.1016/j.epsl.2012.03.033, 2012.

Sasgen, I., Konrad, H., Ivins, E. R., Van den Broeke, M. R., Bamber, J. L., Martinec, Z., and Klemann, V.: Antarctic ice-mass balance 2003 to 2012: regional reanalysis of GRACE satellite gravimetry measurements with improved estimate of glacial-isostatic adjustment based on GPS uplift rates, The Cryosphere, 7, 1499–1512, https://doi.org/10.5194/tc-7-1499-2013, 2013.

Sasgen, I., Konrad, H., Helm, V., and Grosfeld, K.: High-resolution mass trends of the Antarctic Ice Sheet through a spectral combination of satellite gravimetry and radar altimetry observations, Remote Sens., 11, Article 2, https://doi.org/10.3390/rs11020144, 2019.

Sasgen, I., Wouters, B., Gardner, A. S., King, M. D., Tedesco, M., Landerer, F. W., Dahle, C., Save, H., and Fettweis, X.: Return to rapid ice loss in Greenland and record loss in 2019 detected by the GRACE-FO satellites, Commun. Earth Environ., 1, 1–8, https://doi.org/10.1038/s43247-020-0010-1, 2020.

Savcenko, R., Bosch, W., Dettmering, D., and Seitz, F.: EOT11a—Global Empirical Ocean Tide Model from multi-mission satellite altimetry, with links to model results, PANGAEA [data set], https://doi.org/10.1594/PANGAEA.834232, 2012.

Schlaak, M. and Pail, R.: Resolving climate-related mass transport trends: A parameter model comparison using closed-loop simulations of current and future satellite gravity missions, Earth Planets Space, 77, 97, https://doi.org/10.1186/s40623-025-02239-0, 2025.

Schlaak, M., Pfeffer, J., and Pail, R.: Simulated L2 and L3 products for impact studies of the NGGM and MAGIC gravity missions, GFZ Data Services [data set], https://doi.org/10.5880/fidgeo.2026.049, 2026.

Schnaubelt, J. C., Tabor, C. R., Otto-Bliesner, B. L., and Lora, J. M.: Atmospheric River Impacts on the Greenland Ice Sheet Through the Last Interglacial, AGU Adv., 6, e2025AV001653, https://doi.org/10.1029/2025AV001653, 2025.

https://doi.org/10.5194/egusphere-2026-4642
Preprint. Discussion started: 7 August 2026

Slangen, A. B. A., Carson, M., Katsman, C. A., van de Wal, R. S. W., Köhl, A., Vermeersen, L. L. A., and Stammer, D.: Projecting twenty-first century regional sea-level changes, Clim. Change, 124, 317–332, https://doi.org/10.1007/s10584-014-1080-9, 2014.

Spada, G.: Glacial Isostatic Adjustment and Contemporary Sea Level Rise: An Overview, Surv. Geophys., 38, 153–185, https://doi.org/10.1007/s10712-016-9379-x, 2017.

Spada, G. and Melini, D.: On Some Properties of the Glacial Isostatic Adjustment Fingerprints, Water, 11, Article 9, https://doi.org/10.3390/w11091844, 2019.

Tapley, B. D., Bettadpur, S., Ries, J. C., Thompson, P. F., and Watkins, M. M.: GRACE Measurements of Mass Variability in the Earth System, Science, 305, 503–505, https://doi.org/10.126/science.1099192, 2004.

Tapley, B. D., Watkins, M. M., Flechtner, F., Reigber, C., Bettadpur, S., Rodell, M., Sasgen, I., Famiglietti, J. S., Landerer, F. W., Chambers, D. P., Reager, J. T., Gardner, A. S., Save, H., Ivins, E. R., Swenson, S. C., Boening, C., Dahle, C., Wiese, D. N., Dobslaw, H., and Velicogna, I.: Contributions of GRACE to understanding climate change, Nat. Clim. Change, 9, 358–369, https://doi.org/10.1038/s41558-019-0456-2, 2019.

The IMBIE Team: Mass balance of the Greenland Ice Sheet from 1992 to 2018, Nature, 579, 233–239, https://doi.org/10.1038/s41586-019-1855-2, 2020.

Vergos, G. S., Tziavos, I. N., Mertikas, S., Piretzidis, D., Frantzis, X., and Donlon, C.: Local Gravity and Geoid Improvements around the Gavdos Satellite Altimetry Cal/Val Site, Remote Sens., 16, 3243, https://doi.org/10.3390/rs16173243, 2024.

Wahr, J., Molenaar, M., and Bryan, F.: Time variability of the Earth's gravity field: Hydrological and oceanic effects and their possible detection using GRACE, J. Geophys. Res.: Solid Earth, 103, 30205–30229, https://doi.org/10.1029/98JB02844, 1998.

Wouters, B., Gardner, A. S., and Moholdt, G.: Global Glacier Mass Loss During the GRACE Satellite Mission (2002–2016), Front. Earth Sci., 7:96, https://doi.org/10.3389/feart.2019.00096, 2019.

WWF: Water Risk Filter, https://riskfilter.org/water/home (last access:31/07/2026).

Zhao, M., A, G., Velicogna, I., and Kimball, J. S.: A Global Gridded Dataset of GRACE Drought Severity Index for 2002–14: Comparison with PDSI and SPEI and a Case Study of the Australia Millennium Drought, J. Hydrometeorol., 18, 2117–2129, https://doi.org/10.1175/JHM-D-16-0182.1, 2017.